



Yani Zhang · Junlin Li  · Xiufeng Xie

Dynamic analysis of interfacial multiple cracks in piezoelectric thin film/substrate

Received: 29 May 2022 / Revised: 7 October 2022 / Accepted: 8 October 2022 / Published online: 15 November 2022
© The Author(s), under exclusive licence to Springer-Verlag GmbH Austria, part of Springer Nature 2022

Abstract The dynamic fracture characteristics of mode-III cracks are investigated. This is a crucial problem in piezoelectric devices. The theoretical solution to this problem is described using the integral-transform method (Laplace and Fourier transforms) and the Chebyshev point method. A crack-propagation model is provided to obtain the stress and electrical-displacement fields near the crack tips. The results show that crack propagation is related to the electromechanical coupling coefficient and film thickness. The effect of film thickness has not been considered in previous literature. In the case of multiple cracks, according to their mutual effects, the nondimensional DSIF inside the crack tip is more significant than that outside the crack tip, regardless of the number of cracks. When the film thickness is small, the change in the DSIF is significant, indicating appropriate circumstances, and a thinner film thickness is more conducive to safe design. Negative electrical-displacement loads always prevent crack propagation, whereas positive electric-displacement loads can promote or prevent crack propagation. Numerical examples are provided to highlight the result.

1 Introduction

1.1 Background

Owing to their electromechanical coupling behavior, piezoelectric materials have been widely used in advanced instruments. However, fractures can cause safety accidents. Therefore, cracks, which represent their main disadvantages, have been extensively investigated [1–10]. With the emergence of piezoelectric bimetals, the behavior of interfacial cracks has raised significant concerns [11–13].

However, all the above works have focused on static propagation. Recently, many researchers [14, 15] have studied the dynamic fracture of cracks. Narita [16] researched a crack in a piezoelectric layer. The results showed that designing piezoelectric devices was feasible and practical. The DSIF was obtained from Gu [17]. A semi-infinite interfacial crack and permeable cracks between two piezoelectric materials were analyzed [18, 19].

Piezoelectric films and coatings have recently emerged, which allow for the design of more sophisticated materials and devices and expand the range of piezoelectric material applications [20–29].

Piezoelectric thin-film/substrate materials are widely used in modern life. However, due to mismatched characteristics, piezoelectric thin-film/substrate materials tend to fracture at the interface under in-service loading conditions. Nonetheless, most of the abovementioned studies on the fracture of piezoelectric biomaterials

Y. Zhang
School of Materials Science and Engineering, Taiyuan University of Science and Technology, Taiyuan 030024, China

J. Li (✉) · X. Xie
School of Applied Science, Taiyuan University of Science and Technology, Taiyuan 030024, China
e-mail: lijunlin211014@163.com

have been focused on large grain sizes, and a few studies have been conducted on the fracture of micrometer-scale piezoelectric thin films, especially the dynamic analysis of multiple cracks in a piezoelectric thin film/substrate. In addition, stress, thin film thickness, substrate thickness, and impact time play an essential role in the structural safety design of piezoelectric film/substrate. Thus, the investigation of these factors with the dynamic expansion of a piezoelectric film/substrate represents the innovation of the present study.

1.2 Outline

This paper is organized as follows. Section 2 presents in detail the constitutive equations and mixed initial boundary conditions. Section 3 provides the integral equations and calculates the DSIF under anti-plane mechanical stress and electric displacement impact loading. The DSIF under far-field forces and electric impact loading are provided in Sect. 4. The numerical examples are discussed in Sect. 5. The conclusions are provided in Sect. 6.

2 Problem statement and formulation

Figure 1 shows that the piezoelectric thin film and substrate occupy the domains Ω_1 and Ω_2 , respectively. The film and substrate thicknesses are d_1 and d_2 , respectively. Multiple interface cracks appear in the same direction and belong to this interval (a_k, b_k) ($k = 1, 2, \dots, n$), where a_k and b_k denote the left and right ends of the crack, respectively. We assume that the crack is in static equilibrium when $t < 0$. The crack propagation velocity is v . The crack tip is located at $x = vt$ ($t > 0$).

The dynamic anti-plane equilibrium equations of the piezoelectric thin film/substrate are written as

$$c_{44}^{(m)} \left(\frac{\partial^2 w}{\partial X^2} + \frac{\partial^2 w}{\partial Y^2} \right) + e_{15}^{(m)} \left(\frac{\partial^2 \phi}{\partial X^2} + \frac{\partial^2 \phi}{\partial Y^2} \right) = \rho^{(m)} \frac{\partial^2 w}{\partial t^2}, \quad (1)$$

$$e_{15}^{(m)} \left(\frac{\partial^2 w}{\partial X^2} + \frac{\partial^2 w}{\partial Y^2} \right) - \varepsilon_{11}^{(m)} \left(\frac{\partial^2 \phi}{\partial X^2} + \frac{\partial^2 \phi}{\partial Y^2} \right) = 0, \quad (2)$$

where $w = w(x, y, t)$ and $\phi(x, y, t)$ represent the displacement components and the electric dielectric constants, respectively; $\rho^{(m)}$ is the mass density; and $m = 1, 2$ signify the upper and lower materials, respectively.

A moving coordinate system is introduced as

$$x = X - vt, \quad y = Y. \quad (3)$$

By using the transformation, Eq. (1) may be expressed as follows:

$$\left[1 - \left(\frac{v}{\bar{c}_m} \right)^2 \right] \frac{\partial^2 w}{\partial x^2} + \frac{\partial^2 w}{\partial y^2} + \frac{e_{15}^{(m)}}{c_{44}^{(m)}} \left(\frac{\partial^2 \phi}{\partial x^2} + \frac{\partial^2 \phi}{\partial y^2} \right) = \left(\frac{1}{\bar{c}_m} \right)^2 \left(\frac{\partial^2 w}{\partial t^2} - 2v \frac{\partial^2 w}{\partial x \partial t} \right) \quad (4)$$

$$\frac{e_{15}^{(m)}}{c_{44}^{(m)}} \left(\frac{\partial^2 w}{\partial x^2} + \frac{\partial^2 w}{\partial y^2} \right) - \frac{\varepsilon_{11}^{(m)}}{c_{44}^{(m)}} \left(\frac{\partial^2 \phi}{\partial x^2} + \frac{\partial^2 \phi}{\partial y^2} \right) = 0, \quad (5)$$

where $\bar{c}_m = \left(c_{44}^{(m)} / \rho^{(m)} \right)^{\frac{1}{2}}$ is the shear bulk wave velocity.

3 Anti-plane mechanical stress and electric displacement impact loading

The mixed mechanical boundary conditions of the issues become:

$$\tau_{yz}(x, 0^+, t) = \tau_{yz}(x, 0^-, t) = -\tau_0 H(t), \quad x \in (a_k, b_k), \quad (6)$$

$$D_y(x, 0^+, t) = D_y(x, 0^-, t) = -D_0 H(t), \quad x \in (a_k, b_k), \quad (7)$$

$$w(x, 0^+, t) = w(x, 0^-, t), \quad x \notin (a_k, b_k), \quad (8)$$

$$\phi(x, 0^+, t) = \phi(x, 0^-, t), \quad x \notin (a_k, b_k), \quad (9)$$

$$\tau_{yz}(x, 0^+, t) = \tau_{yz}(x, 0^-, t), x \notin (a_k, b_k), \tag{10}$$

$$D_y(x, 0^+, t) = D_y(x, 0^-, t), x \notin (a_k, b_k), \tag{11}$$

$$w(x, y^+, t) = w(x, y^-, t) = 0, x^2 + y^2 \rightarrow \infty, \tag{12}$$

$$\phi(x, y^+, t) = \phi(x, y^-, t) = 0, x^2 + y^2 \rightarrow \infty, \tag{13}$$

$$\tau_{yz}(x, d_1, t) = \tau_{yz}(x, -d_2, t) = 0, \tag{14}$$

$$D_y(x, d_1, t) = D_y(x, -d_2, t) = 0, \tag{15}$$

where D_0 is the electric displacement, τ_0 is the stress, and $H(t) = \begin{cases} 0, & t < 0, \\ 1, & t > 0. \end{cases}$

We assume that the piezoelectric biomaterials are at mechanical and electrical rest at $t = 0$, which is

$$w(x, y, 0) = 0, \frac{\partial w(x, y, 0)}{\partial t} = 0, -\infty < x, y < +\infty. \tag{16}$$

$$\phi(x, y, 0) = 0, \frac{\partial \phi(x, y, 0)}{\partial t} = 0, -\infty < x, y < +\infty. \tag{17}$$

Following Li and Mataga [14, 15], a function is written as

$$\varphi = \phi - \frac{e_{15}^{(m)}}{\varepsilon_{11}^{(m)}} w. \tag{18}$$

3.1 Solution to the problem

The Fourier transform on x and Laplace transform on t , we obtain [30]

$$w^*(\zeta, y, p) = \int_{-\infty}^{+\infty} \int_0^{+\infty} w(x, y, t) e^{-pt} dt e^{i\zeta x} dx, \tag{19}$$

$$\phi^*(\zeta, y, p) = \int_{-\infty}^{+\infty} \int_0^{+\infty} \phi(x, y, t) e^{-pt} dt e^{i\zeta x} dx, \tag{20}$$

$$\varphi^*(\zeta, y, p) = \int_{-\infty}^{+\infty} \int_0^{+\infty} \phi(x, y, t) e^{-pt} dt e^{i\zeta x} dx - \frac{e_{15}^{(m)}}{\varepsilon_{11}^{(m)}} \int_{-\infty}^{+\infty} \int_0^{+\infty} w(x, y, t) e^{-pt} dt e^{i\zeta x} dx, \tag{21}$$

where $\zeta = \zeta_1 + i\zeta_2$ is complex.

According to the theory at infinity, we obtain the expression

$$w^*(x, y, p) = \frac{1}{2\pi} \int_{-\infty}^{+\infty} (A_{1m} e^{\alpha_m y} + B_{1m} e^{-\alpha_m y}) e^{-i\zeta x} d\zeta, \tag{22}$$

$$\phi^*(x, y, p) = \frac{e_{15}^{(m)}}{\varepsilon_{11}^{(m)}} w^*(x, y, p) + \frac{1}{2\pi} \int_{-\infty}^{+\infty} (A_{2m} e^{|\zeta|y} + B_{2m} e^{-|\zeta|y}) e^{-i\zeta x} d\zeta, \tag{23}$$

where $\alpha_m(\zeta) = \sqrt{\frac{[f_m - (\frac{v}{c_m})^2]\zeta^2 + \frac{p^2}{c_m^2} + \frac{2vip\zeta}{c_m^2}}{f_m}} = s_k \sqrt{\zeta - ip/(c_m + v)} \sqrt{\zeta + ip/(c_m - v)} = a_{m+}(\zeta) a_{m-}(\zeta)$, $s_m = \sqrt{1 - (v/c_m)^2}$, $f_m = 1 + \frac{e_{15}^{(m)} e_{15}^{(m)}}{c_{44}^{(m)} \varepsilon_{11}^{(m)}}$, A_{1m} and B_{1m} are unknown functions satisfying the loading displacement $w^*(x, y, p)$, and A_{2m} and B_{2m} are unknown functions satisfying the electric field $\phi^*(x, y, p)$.

The boundary conditions, i.e., Eqs. (6–15), can be assumed to take the form

$$\tau_{yz}^*(x, 0^+, p) = \tau_{yz}^*(x, 0^-, p) = -\frac{\tau_0}{p}, x \in (a_k, b_k), \tag{24}$$

$$D_y^*(x, 0^+, p) = D_y^*(x, 0^-, p) = -\frac{D_0}{p}, \quad x \in (a_k, b_k), \quad (25)$$

$$w^*(x, 0^+, p) = w^*(x, 0^-, p), \quad x \notin (a_k, b_k), \quad (26)$$

$$\varphi^*(x, 0^+, p) = \varphi^*(x, 0^-, p), \quad x \notin (a_k, b_k), \quad (27)$$

$$\tau_{yz}^*(x, 0^+, p) = \tau_{yz}^*(x, 0^-, p), \quad x \notin (a_k, b_k), \quad (28)$$

$$D_y^*(x, 0^+, p) = D_y^*(x, 0^-, p), \quad x \notin (a_k, b_k), \quad (29)$$

$$\tau_{yz}^*(x, d_1, p) = \tau_{yz}^*(x, -d_2, p) = 0, \quad (30)$$

$$D_y^*(x, d_1, p) = D_y^*(x, -d_2, p) = 0. \quad (31)$$

According to the geometric equation [28], we have:

$$\begin{aligned} \tau_{yz}^*(x, y, p) &= c_{44}^{(m)} \frac{\partial w}{\partial y} + e_{15}^{(m)} \frac{\partial \phi}{\partial y} \\ &= \frac{1}{2\pi} \int_{-\infty}^{+\infty} c_{44}^{(m)} \left(1 + \frac{e_{15}^{(m)} e_{15}^{(m)}}{\varepsilon_{11}^{(m)}} \right) (A_{1m} \alpha_m e^{\alpha_m y} - B_{1m} \alpha_m e^{-\alpha_m y}) e^{-i\zeta x} d\zeta \\ &\quad + \frac{1}{2\pi} \int_{-\infty}^{+\infty} e_{15}^{(m)} (A_{2m} |\zeta| e^{|\zeta| y} - B_{2m} |\zeta| e^{-|\zeta| y}) e^{-i\zeta x} d\zeta, \end{aligned} \quad (32)$$

$$D_y^*(x, y, p) = -\varepsilon_{11}^{(m)} \frac{1}{2\pi} \int_{-\infty}^{+\infty} (A_{2m} |\zeta| e^{|\zeta| y} - B_{2m} |\zeta| e^{-|\zeta| y}) e^{-i\zeta x} d\zeta. \quad (33)$$

Substituting Eqs. (28–31) into Eqs. (32–33), respectively, we obtain:

$$c_{44}^{(1)} \left(1 + \frac{e_{15}^{(1)} e_{15}^{(1)}}{\varepsilon_{11}^{(1)}} \right) \alpha_1 (A_{11} e^{\alpha_1 d_1} - B_{11} e^{-\alpha_1 d_1}) + e_{15}^{(1)} |\zeta| (A_{21} e^{|\zeta| d_1} - B_{21} e^{-|\zeta| d_1}) = 0, \quad (34)$$

$$c_{44}^{(2)} \left(1 + \frac{e_{15}^{(2)} e_{15}^{(2)}}{\varepsilon_{11}^{(2)}} \right) a_2 (A_{12} e^{-a_2 d_2} - B_{12} e^{a_2 d_2}) + e_{15}^{(2)} |\zeta| (A_{22} e^{-|\zeta| d_2} - B_{22} e^{|\zeta| d_2}) = 0, \quad (35)$$

$$-\varepsilon_{11}^{(1)} |\zeta| (A_{21} e^{|\zeta| d_1} - B_{21} e^{-|\zeta| d_1}) = 0, \quad (36)$$

$$-\varepsilon_{11}^{(2)} |\zeta| (A_{22} e^{-|\zeta| d_2} - B_{22} e^{|\zeta| d_2}) = 0, \quad (37)$$

$$\begin{aligned} c_{44}^{(1)} \left(1 + \frac{e_{15}^{(1)} e_{15}^{(1)}}{\varepsilon_{11}^{(1)}} \right) a_1 (A_{11} - B_{11}) + e_{15}^{(1)} |\zeta| (A_{21} - B_{21}) \\ = c_{44}^{(2)} \left(1 + \frac{e_{15}^{(2)} e_{15}^{(2)}}{\varepsilon_{11}^{(2)}} \right) a_2 (A_{12} - B_{12}) + e_{15}^{(2)} |\zeta| (A_{22} - B_{22}), \end{aligned} \quad (38)$$

$$-\varepsilon_{11}^{(1)} |\zeta| (A_{21} - B_{21}) = -\varepsilon_{11}^{(2)} |\zeta| (A_{22} - B_{22}). \quad (39)$$

According Eqs. (34–39), we have:

$$A_{21} = B_{21} e^{-2|\zeta| d_1}, \quad B_{22} = A_{22} e^{-2|\zeta| d_2}, \quad A_{11} = B_{11} e^{-2\alpha_1 d_1}, \quad B_{12} = A_{12} e^{-2\alpha_2 d_2}, \quad (40)$$

$$B_{21} = \frac{\varepsilon_{11}^{(2)} (1 - e^{-2|\zeta| d_2})}{\varepsilon_{11}^{(1)} (1 - e^{-2|\zeta| d_1})} B_{22}, \quad B_{21} = -\frac{\varepsilon_{11}^{(2)} (1 - e^{-2|\zeta| d_2})}{\varepsilon_{11}^{(1)} (1 - e^{-2|\zeta| d_1})} A_{22}. \quad (41)$$

This problem is solved more efficiently by using the continuous distribution function to simulate collinear cracks. The density function is introduced as follows:

$$h_{w^{(k)}}(x) = \frac{d}{dx} [w^{(k)}(x, 0^+, p) - w^{(k)}(x, 0^-, p)], \quad k = 1, 2, \dots, n, \quad (42)$$

$$h_{\varphi^{(k)}}(x) = \frac{d}{dx} [\varphi^{(k)}(x, 0^+, p) - \varphi^{(k)}(x, 0^-, p)], \quad k = 1, 2, \dots, n. \quad (43)$$

Substituting Eqs. (26–27) into Eqs. (42–43), respectively, we have [10]:

$$A_{11} + B_{11} - A_{12} - B_{12} = \frac{i}{\zeta} \int_{a_k}^{b_k} h_{w(k)}(s)e^{i\zeta s} ds = \eta_1, \tag{44}$$

$$\frac{e_{15}^{(1)}}{\varepsilon_{11}^{(1)}}(A_{11} + B_{11}) - \frac{e_{15}^{(2)}}{\varepsilon_{11}^{(2)}}(A_{12} + B_{12}) + (A_{21} + B_{21} - A_{22} - B_{22}) = \frac{i}{\xi} \int_{a_k}^{b_k} h_{\varphi(k)}(s)e^{i\xi s} ds = \eta_2. \tag{45}$$

Solving Eqs. (40–41) and Eqs. (44–45), we obtain:

$$A_{11} = \frac{R_1\eta_1 + R_2\eta_2}{R}, B_{11} = \frac{R_3\eta_1 + R_4\eta_2}{R}, A_{12} = \frac{R_5\eta_1 + R_6\eta_2}{R}, B_{12} = \frac{R_7\eta_1 + R_8\eta_2}{R}, \tag{46}$$

$$A_{21} = \frac{R_9\eta_1 + R_{10}\eta_2}{R}, B_{21} = \frac{R_{11}\eta_1 + R_{12}\eta_2}{R}, A_{22} = \frac{R_{13}\eta_1 + R_{14}\eta_2}{R}, B_{22} = \frac{R_{15}\eta_1 + R_{16}\eta_2}{R}. \tag{47}$$

The values of R and R_n ($n = 1, 2, \dots, 16$) are given in the Appendix.

The unknown functions A_{1m}, A_{2m}, B_{1m} and B_{2m} ($m = 1, 2$) depend on η_1, η_2 . If we determine the values of η_1 and η_2 , then we can obtain the stress and electric displacement expressions. We know that the values of η_1 and η_2 rely on the density functions $h_{w(k)}$, and $h_{\varphi(k)}$ ($k = 1, 2, 3 \dots, n$). Therefore, we need to solve for the density function $h_{w(k)}$, and $h_{\varphi(k)}$ ($k = 1, 2, 3 \dots, n$).

Using Eqs. (32–33) and Eqs. (42–43), the equation expressions of the upper half plane are:

$$\begin{aligned} & \frac{1}{2\pi} \int_{-\infty}^{+\infty} p_1 \frac{i\alpha_1 e^{\alpha_1 y}}{R\zeta} \left[(R_1 - R_3) \int_{a_k}^{b_k} h_{w(k)}(s)e^{i\zeta s} ds + (R_2 - R_4) \int_{a_k}^{b_k} h_{\varphi(k)}(s)e^{i\zeta s} ds \right] e^{-i\zeta x} d\zeta \\ & + \frac{1}{2\pi} \int_{-\infty}^{+\infty} e_{15}^{(1)} \frac{i|\zeta| e^{\alpha_1 y}}{R\zeta} \left[(R_9 - R_{11}) \int_{a_k}^{b_k} h_{w(k)}(s)e^{i\zeta s} ds + (R_{10} - R_{12}) \int_{a_k}^{b_k} h_{\varphi(k)}(s)e^{i\zeta s} ds \right] e^{-i\zeta x} d\zeta \\ & = \frac{1}{2\pi} \int_{a_k}^{b_k} \left[\int_{-\infty}^{+\infty} p_1 (R_1 - R_3) \frac{i\alpha_1 e^{\alpha_1 y}}{R\zeta} e^{i\zeta(s-x)} d\zeta \right] h_{w(k)}(s) ds \\ & + \frac{1}{2\pi} \int_{a_k}^{b_k} \left[\int_{-\infty}^{+\infty} p_1 (R_2 - R_4) \frac{i\alpha_1 e^{\alpha_1 y}}{R\zeta} e^{i\zeta(s-x)} d\zeta \right] h_{\varphi(k)}(s) ds \\ & + \frac{1}{2\pi} \int_{a_k}^{b_k} \left[\int_{-\infty}^{+\infty} e_{15}^{(1)} (R_9 - R_{11}) \frac{i|\zeta| e^{\alpha_1 y}}{R\zeta} e^{i\zeta(s-x)} d\zeta \right] h_{w(k)}(s) ds \\ & + \frac{1}{2\pi} \int_{a_k}^{b_k} \left[\int_{-\infty}^{+\infty} e_{15}^{(1)} (R_{10} - R_{12}) \frac{i|\zeta| e^{\alpha_1 y}}{R\zeta} e^{i\zeta(s-x)} d\zeta \right] h_{\varphi(k)}(s) ds \\ & = -\frac{\tau_0}{p}, \end{aligned} \tag{48}$$

$$\begin{aligned} & -\frac{1}{2\pi} \int_{a_k}^{b_k} \left[\int_{-\infty}^{+\infty} \varepsilon_{11}^{(1)} (R_9 - R_{11}) \frac{i|\zeta| e^{|\zeta| y}}{R\zeta} e^{i\zeta(s-x)} d\zeta \right] h_{w(k)}(s) ds \\ & -\frac{1}{2\pi} \int_{a_k}^{b_k} \left[\int_{-\infty}^{+\infty} \varepsilon_{11}^{(1)} (R_{10} - R_{12}) \frac{i|\zeta| e^{|\zeta| y}}{R\zeta} e^{i\zeta(s-x)} d\zeta \right] h_{\varphi(k)}(s) ds \\ & = -\frac{D_0}{p}, \end{aligned} \tag{49}$$

where $p_1 = c_{44}^{(1)} \left(1 + \frac{e_{15}^{(1)} e_{15}^{(1)}}{\varepsilon_{11}^{(1)}} \right)$

Now, we transform Eqs. (48) and (49) into the integral Cauchy nuclear equation of the first kind:

$$\begin{aligned} & \frac{1}{2\pi} \int_{a_k}^{b_k} \left[\int_{-\infty}^{+\infty} H_1 \frac{i\alpha_1 e^{\alpha_1 y}}{R\zeta} e^{i\zeta(s-x)} d\zeta \right] h_{w(k)}(s) ds + \frac{1}{2\pi} \int_{a_k}^{b_k} \left[\int_{-\infty}^{+\infty} H_2 \frac{i\alpha_1 e^{\alpha_1 y}}{R\zeta} e^{i\zeta(s-x)} d\zeta \right] h_{\varphi(k)}(s) ds \\ & + \frac{1}{2\pi} \int_{a_k}^{b_k} \left[\int_{-\infty}^{+\infty} H_3 \frac{i|\zeta| e^{\alpha_1 y}}{R\zeta} e^{i\zeta(s-x)} d\zeta \right] h_{w(k)}(s) ds + \frac{1}{2\pi} \int_{a_k}^{b_k} \left[\int_{-\infty}^{+\infty} H_4 \frac{i|\zeta| e^{\alpha_1 y}}{R\zeta} e^{i\zeta(s-x)} d\zeta \right] h_{\varphi(k)}(s) ds \\ & = -\frac{\tau_0}{p}, \end{aligned} \tag{50}$$

$$\begin{aligned}
 & -\frac{1}{2\pi} \int_{a_k}^{b_k} \left[\int_{-\infty}^{+\infty} H_5 \frac{i|\zeta|e^{|\zeta|y}}{R\zeta} e^{i\zeta(s-x)} d\zeta \right] h_{w(k)}(s) ds - \frac{1}{2\pi} \int_{a_k}^{b_k} \left[\int_{-\infty}^{+\infty} H_6 \frac{i|\zeta|e^{|\zeta|y}}{R\zeta} e^{i\zeta(s-x)} d\zeta \right] h_{\varphi(k)}(s) ds \\
 & = -\frac{D_0}{p},
 \end{aligned} \tag{51}$$

where $p_1(R_1 - R_3) = H_1$, $p_1(R_2 - R_4) = H_2$, $e_{15}^{(1)}(R_9 - R_{11}) = H_3$, $e_{15}^{(1)}(R_{10} - R_{12}) = H_4$, $\varepsilon_{11}^{(1)}(R_9 - R_{11}) = H_5$, $\varepsilon_{11}^{(1)}(R_{10} - R_{12}) = H_6$.

On the crack surface, we have:

$$\int_{a_k}^{b_k} \left(\int_{-\infty}^{+\infty} \frac{H_1^*}{R^*} \frac{1}{s-x} + h_1(x, s) \right) h_{w(k)}(s) ds + \int_{a_k}^{b_k} \left(\int_{-\infty}^{+\infty} \frac{H_2^*}{R^*} \frac{1}{s-x} + h_2(x, s) \right) h_{\varphi(k)}(s) ds = -\pi \frac{\tau_0}{p}, \tag{52}$$

$$\int_{a_k}^{b_k} \left(\int_{-\infty}^{+\infty} \frac{H_3^*}{R^*} \frac{1}{s-x} + h_3(x, s) \right) h_{w(k)}(s) ds + \int_{a_k}^{b_k} \left(\int_{-\infty}^{+\infty} \frac{H_4^*}{R^*} \frac{1}{s-x} + h_4(x, s) \right) h_{\varphi(k)}(s) ds = -\pi \frac{D_0}{p}, \tag{53}$$

where

$$\begin{aligned}
 H_1^* &= s_1 p_1 \left(s_2 p_2 \frac{\varepsilon_{11}^{(2)}}{\varepsilon_{11}^{(1)}} - \frac{e_{15}^{(2)} e_{15}^{(2)} \varepsilon_{11}^{(2)} - e_{15}^{(1)} \varepsilon_{11}^{(1)}}{\varepsilon_{11}^{(2)} \varepsilon_{11}^{(1)}} \right) - e_{15}^{(1)} \frac{\varepsilon_{11}^{(2)}}{\varepsilon_{11}^{(1)}} \left(s_2 p_2 \frac{e_{15}^{(1)}}{\varepsilon_{11}^{(1)}} + s_1 p_1 \frac{e_{15}^{(2)}}{\varepsilon_{11}^{(2)}} \right), \\
 H_2^* &= -s_1 p_1 \frac{e_{15}^{(2)} \varepsilon_{11}^{(1)} - e_{15}^{(1)} \varepsilon_{11}^{(2)}}{\varepsilon_{11}^{(1)}} - e_{15}^{(1)} \frac{\varepsilon_{11}^{(2)}}{\varepsilon_{11}^{(1)}} (s_2 p_2 + s_1 p_1), \\
 H_3^* &= \varepsilon_{11}^{(2)} \left(s_2 p_2 \frac{e_{15}^{(1)}}{\varepsilon_{11}^{(1)}} + s_1 p_1 \frac{e_{15}^{(2)}}{\varepsilon_{11}^{(2)}} \right), \\
 H_4^* &= \varepsilon_{11}^{(2)} (s_2 p_2 + s_1 p_1), \\
 R^* &= -\frac{(e_{15}^{(1)} \varepsilon_{11}^{(2)} - e_{15}^{(2)} \varepsilon_{11}^{(1)})^2}{\varepsilon_{11}^{(1)} \varepsilon_{11}^{(1)} \varepsilon_{11}^{(2)}} + \frac{\varepsilon_{11}^{(2)}}{\varepsilon_{11}^{(1)}} (s_2 p_2 + s_1 p_1), \\
 h_1(x, s) &= \int_0^\infty \left(\frac{H_1 + H_3}{R} - \frac{H_1^*}{R^*} \right) \sin(\zeta(s-x)) d\zeta, \\
 h_2(x, s) &= \int_0^\infty \left(\frac{H_2 + H_4}{R} - \frac{H_2^*}{R^*} \right) \sin(\zeta(s-x)) d\zeta, \\
 h_3(x, s) &= \int_0^\infty \left(\frac{H_5}{R} - \frac{H_3^*}{R^*} \right) \sin(\zeta(s-x)) d\zeta, \\
 h_4(x, s) &= \int_0^\infty \left(\frac{H_6}{R} - \frac{H_4^*}{R^*} \right) \sin(\zeta(s-x)) d\zeta.
 \end{aligned} \tag{54}$$

Considering the boundary conditions and superposition principle, Eqs. (52) and (53) can be expressed as:

$$\begin{aligned}
 & \sum_{k=1}^n \left(\int_{a_k}^{b_k} \left(\frac{H_1^*}{R^*} \frac{1}{s_k - x_j} + h_1(x_j, s_k) \right) h_{w(k)}(s_k) ds_k + \int_{a_k}^{b_k} \left(\frac{H_2^*}{R^*} \frac{1}{s_k - x_j} + h_2(x_j, s_k) \right) h_{\varphi(k)}(s_k) ds_k \right) \\
 & = -\pi \frac{\tau_0}{p}, \quad x_j \in (a_j, b_j), j, k = 1, 2, \dots, n,
 \end{aligned} \tag{55}$$

$$\begin{aligned}
 & \sum_{k=1}^n \left(\int_{a_k}^{b_k} \left(\frac{H_3^*}{R^*} \frac{1}{s_k - x_j} + h_3(x_j, s_k) \right) h_{w(k)}(s_k) ds_k + \int_{a_k}^{b_k} \left(\frac{H_4^*}{R^*} \frac{1}{s_k - x_j} + h_4(x_j, s_k) \right) h_{\varphi(k)}(s_k) ds_k \right) \\
 & = -\frac{1}{\varepsilon_{11}^{(1)}} \frac{D_0}{p}, \quad x_j \in (a_j, b_j), j, k = 1, 2, \dots, n.
 \end{aligned} \tag{56}$$

By transforming, we have:

$$h_{w(k)}(x) = g_{1(k)}(x),$$

$$h_{\varphi^{(k)}}(x) = g_{2^{(k)}}(x),$$

$$h_i(x, s) = P_i(f, l), \quad (i = 1, 2, 3, 4).$$

For the convenience and accuracy of numerical calculation, the normalized quantities are defined as:

$$m_{o_k} = \frac{b_k - a_k}{2}, \quad n_{o_k} = \frac{b_k + a_k}{2} \quad (k = 1, 2, \dots, n), \quad (57)$$

$$f_k = \frac{x_k - n_{o_k}}{m_{o_k}}, \quad l_k = \frac{s_k - n_{o_k}}{m_{o_k}} \quad (k = 1, 2, \dots, n). \quad (58)$$

Using equations (57) and (58), the integral equations (55) and (56) can be expressed as follows:

$$\begin{aligned} & \sum_{k=1}^n \int_{-1}^1 \left(\frac{H_1^*}{R^*} \frac{m_{o_k}}{m_{o_k} l_k + n_{o_k} - m_{o_j} f_j - n_{o_j}} + m_{o_k} P_1(f_j, l_k) \right) g_{1^{(k)}}(l_k) dl_k \\ & + \sum_{k=1}^n \int_{-1}^1 \left(\frac{H_2^*}{R^*} \frac{m_{o_j}}{m_{o_k} l_k + n_{o_k} - m_{o_j} f_j - n_{o_j}} + m_{o_k} P_2(f_j, l_k) \right) g_{2^{(k)}}(l_k) dl_k = -\pi \frac{\tau_0}{p}, \end{aligned} \quad (59)$$

$$\begin{aligned} & \sum_{k=1}^n \int_{-1}^1 \left(\frac{H_3^*}{R^*} \frac{m_{o_k}}{m_{o_k} l_k + n_{o_k} - m_{o_j} f_j - n_{o_j}} + m_{o_k} P_3(f_j, l_k) \right) g_{1^{(k)}}(l_k) dl_k + \\ & \sum_{k=1}^n \int_{-1}^1 \left(\frac{H_4^*}{R^*} \frac{m_{o_j}}{m_{o_k} l_k + n_{o_k} - m_{o_j} f_j - n_{o_j}} + m_{o_k} P_4(f_j, l_k) \right) g_{2^{(k)}}(l_k) dl_k = -\frac{\pi D_0}{p}. \end{aligned} \quad (60)$$

To obtain the dislocation densities on the surface of the interface crack, we need to solve the Cauchy singular integral equation. We can observe that the dominant part of the integral equation has a Cauchy kernel. We find that the dislocation density functions $g_{1^{(k)}}(l_k)$ and $g_{2^{(k)}}(l_k)$ ($k = 1, 2, \dots, n$) in Eqs. (59) and (60) have square-root type singularities. We can express that $g_{1^{(k)}}(l_k) = (1/\sqrt{1-l_k^2}) \cdot h_{1^{(k)}}(l_k) \pi \tau_0 \cdot (1/p)$, where $h_{1^{(k)}}(l_k)$ is a continuous function defined in the interval $[-1, 1]$. Therefore, the following equations are obtained:

$$g_{1^{(k)}}(l_k) = \frac{h_{1^{(k)}}(l_k)}{\sqrt{1-l_k^2}} \pi \frac{\tau_0}{p}, \quad (61)$$

$$g_{2^{(k)}}(l_k) = \frac{h_{2^{(k)}}(l_k)}{\sqrt{1-l_k^2}} \pi \frac{D_0}{p}. \quad (62)$$

According to the Chebyshev point method, Eqs. (59) and (60) can be transformed into the following algebraic equation:

$$\begin{aligned} & \frac{1}{N} \sum_{Q=0}^N \chi_Q \sum_{k=1}^n \left(\left(\frac{H_1^*}{R^*} \frac{m_{o_k}}{m_{o_k} l_{kQ} + n_{o_k} - m_{o_j} f_{jq} - n_{o_j}} + m_{o_k} P_1(f_{jq}, l_{kQ}) \right) h_{1^{(k)}}(l_{kQ}) \right. \\ & \left. + \left(\frac{H_2^*}{R^*} \frac{m_{o_k}}{m_{o_k} l_{kQ} + n_{o_k} - m_{o_j} f_{jq} - n_{o_j}} + m_{o_k} P_2(f_{jq}, l_{kQ}) \right) h_{2^{(k)}}(l_{kQ}) \right) = -1, \end{aligned} \quad (63)$$

$$\begin{aligned} & \frac{1}{N} \sum_{Q=0}^N \chi_Q \sum_{k=1}^n \left(\left(\frac{H_3^*}{R^*} \frac{m_{o_k}}{m_{o_k} l_{kQ} + n_{o_k} - m_{o_j} f_{jq} - n_{o_j}} + m_{o_k} P_3(f_{jq}, l_{kQ}) \right) h_{1^{(k)}}(l_{kQ}) \right. \\ & \left. + \left(\frac{H_4^*}{R^*} \frac{m_{o_k}}{m_{o_k} l_{kQ} + n_{o_k} - m_{o_j} f_{jq} - n_{o_j}} + m_{o_k} P_4(f_{jq}, l_{kQ}) \right) h_{2^{(k)}}(l_{kQ}) \right) = -1, \end{aligned} \quad (64)$$

$$\sum_{Q=0}^N \chi_Q h_{1^{(k)}}(l_{kQ}) = 0, \quad \sum_{Q=0}^N \chi_Q h_{2^{(k)}}(l_{kQ}) = 0, \quad j = 1, 2, \dots, n, q = 1, 2, \dots, N, \quad (65)$$

where $\chi_0 = \chi_N = \frac{1}{2}$, $\chi_1 = \dots = \chi_{N-1} = 1$,

$$f_{jq} = \cos \frac{(2q-1)\pi}{2N}, \quad l_{kQ} = \cos \frac{Q\pi}{N}.$$

N is the number of nodes in the quadrature formula. f_{jq} and l_{kQ} are zero points of Chebyshev polynomials of the first and second kinds, respectively. According to Eqs. (63–65), we can find the solutions of $h_{1(k)}(l_k)$ and $h_{2(k)}(l_k)$, so that the stress and electrical displacement are obtained.

3.2 Intensity factors

According to fracture theory, when the DSIF reaches the fracture toughness, the crack will expand, otherwise, the crack will not expand or stop growing. Therefore, it is essential to calculate the DSIF accurately.

According to [31, 32], the DSIF K_{III} and electric displacement intensity factors K_{IV} are expressed as

$$K_{III}^*(a_k) = \sqrt{2\pi(a_k - x)}_{x \rightarrow a_k - 0} \tau_{yz}(x, 0, p), \quad (66)$$

$$K_{IV}^*(a_k) = \sqrt{2\pi(a_k - x)}_{x \rightarrow a_k - 0} D_y(x, 0, p), \quad (67)$$

$$K_{III}^*(b_k) = \sqrt{2\pi(x - b_k)}_{x \rightarrow b_k + 0} \tau_{yz}(x, 0, p), \quad (68)$$

$$K_{IV}^*(b_k) = \sqrt{2\pi(x - b_k)}_{x \rightarrow b_k + 0} D_y(x, 0, p). \quad (69)$$

According to Eqs. (59–62), we have:

$$\lim_{x \rightarrow a_k^-} \tau_{yz}(x, 0, p) = \frac{\tau_0 H_1^*}{pR^*} \lim_{l_k \rightarrow -1^-} \frac{h_{1(k)}(-1)}{\sqrt{l_k^2 - 1}} + \frac{\tau_0 H_2^*}{pR^*} \lim_{l_k \rightarrow -1^-} \frac{h_{2(k)}(-1)}{\sqrt{l_k^2 - 1}}, \quad (70)$$

$$\lim_{x \rightarrow a_k^-} D_y(x, 0, p) = \frac{D_0 H_3^*}{pR^*} \lim_{l_k \rightarrow -1^-} \frac{h_{1(k)}(-1)}{\sqrt{l_k^2 - 1}} + \frac{D_0 H_4^*}{pR^*} \lim_{l_k \rightarrow -1^-} \frac{h_{2(k)}(-1)}{\sqrt{l_k^2 - 1}}, \quad (71)$$

$$\lim_{x \rightarrow b_k^+} \tau_{yz}(x, 0, p) = \frac{\tau_0 H_1^*}{pR^*} \lim_{l_k \rightarrow 1^+} \frac{-h_{1(k)}(1)}{\sqrt{l_k^2 - 1}} + \frac{\tau_0 H_2^*}{pR^*} \lim_{l_k \rightarrow 1^+} \frac{-h_{2(k)}(1)}{\sqrt{l_k^2 - 1}}, \quad (72)$$

$$\lim_{x \rightarrow b_k^+} D_y(x, 0, p) = \frac{D_0 H_3^*}{pR^*} \lim_{l_k \rightarrow 1^+} \frac{-h_{1(k)}(1)}{\sqrt{l_k^2 - 1}} + \frac{D_0 H_4^*}{pR^*} \lim_{l_k \rightarrow 1^+} \frac{-h_{2(k)}(1)}{\sqrt{l_k^2 - 1}}. \quad (73)$$

Using the inverse Laplace transform, we have:

$$K_{III}(a_k) = \tau_0 \sqrt{\pi a_k} (Z_{1k}(t) + Z_{2k}(t)), \quad (74)$$

$$K_{IV}(a_k) = D_0 \sqrt{\pi a_k} (Z_{3k}(t) + Z_{4k}(t)), \quad (75)$$

$$K_{III}(b_k) = -\tau_0 \sqrt{\pi b_k} (Z_{5k}(t) + Z_{6k}(t)), \quad (76)$$

$$K_{IV}(a_k) = -D_0 \sqrt{\pi b_k} (Z_{7k}(t) + Z_{8k}(t)), \quad (77)$$

where

$$Z_{1k}(t) = \frac{1}{2\pi i} \int_{Br} \frac{H_1^*}{pR^*} h_{1(k)}(-1) e^{pt} dp, \quad Z_{2k}(t) = \frac{1}{2\pi i} \int_{Br} \frac{H_2^*}{pR^*} h_{2(k)}(-1) e^{pt} dp,$$

$$Z_{3k}(t) = \frac{1}{2\pi i} \int_{Br} \frac{H_3^*}{pR^*} h_{1(k)}(-1) e^{pt} dp, \quad Z_{4k}(t) = \frac{1}{2\pi i} \int_{Br} \frac{H_4^*}{pR^*} h_{2(k)}(-1) e^{pt} dp,$$

$$Z_{5k}(t) = \frac{1}{2\pi i} \int_{Br} \frac{H_1^*}{pR^*} h_{1(k)}(1) e^{pt} dp, \quad Z_{6k}(t) = \frac{1}{2\pi i} \int_{Br} \frac{H_2^*}{pR^*} h_{2(k)}(1) e^{pt} dp, \quad Z_{7k}(t) = \frac{1}{2\pi i} \int_{Br} \frac{H_3^*}{pR^*} h_{1(k)}(1) e^{pt} dp, \quad Z_{8k}(t) = \frac{1}{2\pi i} \int_{Br} \frac{H_4^*}{pR^*} h_{2(k)}(1) e^{pt} dp.$$

When $t \rightarrow \infty$, according to Eqs. (74–77), we have:

$$K_{III}(a_k) = \tau_0 \sqrt{\pi a_k} \left[\frac{H_1^*}{R^*} h_{1(k)}(-1) + \frac{H_2^*}{R^*} h_{2(k)}(-1) \right], \tag{78}$$

$$K_{IV}(a_k) = D_0 \sqrt{\pi a_k} \left[\frac{H_3^*}{R^*} h_{1(k)}(-1) + \frac{H_4^*}{R^*} h_{2(k)}(-1) \right], \tag{79}$$

$$K_{III}(b_k) = -\tau_0 \sqrt{\pi b_k} \left[\frac{H_1^*}{R^*} h_{1(k)}(1) + \frac{H_2^*}{R^*} h_{2(k)}(1) \right], \tag{80}$$

$$K_{IV}(b_k) = -D_0 \sqrt{\pi b_k} \left[\frac{H_3^*}{R^*} h_{1(k)}(1) + \frac{H_4^*}{R^*} h_{2(k)}(1) \right]. \tag{81}$$

The nondimensional DSIF and electric displacement factors can be expressed as

$$f(v) = K_{III}(t, v) / K_{III}(t, 0) \tag{82}$$

$$g(v) = K_{IV}(t, v) / K_{IV}(t, 0) \tag{83}$$

where $K_{III}(t, v)$ and $K_{IV}(t, v)$ are the universal function for the DSIF and electric displacement intensity factor, respectively; $K_{III}(t, 0)$ and $K_{IV}(t, 0)$ are the DSIF and electric displacement intensity factor for a stationary crack, respectively.

4 Far-field forces and electric impact loading

For piezoelectric media, the boundary conditions of the crack are well-known. The solution to a piezoelectric crack problem involves a geometrically and physically discontinuous problem, and the actual electrical boundary condition should be that the normal electrical displacement of the media is equal to the nondimensional electrical displacement of the defect interface. However, few solutions can be obtained under these boundary conditions. Therefore, according to different defects, they can be divided into impermeable cracks and permeable cracks after approximate treatment.

The nondimensional electrical displacements on the upper and lower surfaces of the crack are considered permeable cracks. The surface charge of an impermeable crack is considered to be zero, which is defined as the D-P boundary condition.

The crack growth problem under stress and electric displacement impact loading ($\tau_\infty H(t)$ and $D_\infty H(t)$) at infinity is investigated. The boundary conditions of Eqs. (6) and (7) are changed into

$$\tau_{yz}(x, 0^+, t) = \tau_{yz}(x, 0^-, t) = -\tau_\infty H(t), \quad x \in (a_k, b_k), \tag{84}$$

$$D_y(x, 0^+, t) = D_y(x, 0^-, t) = D^* - D_\infty H(t), \quad x \in (a_k, b_k), \tag{85}$$

where $H(t) = \begin{cases} 0, & t < 0, \\ 1, & t > 0, \end{cases}$ D^* is the electrical displacement in the crack plane.

Taking the Laplace transform of Eqs. (84) and (85), we obtain

$$\tau_{yz}^*(x, 0^+, p) = \tau_{yz}^*(x, 0^-, p) = -\frac{\tau_\infty}{p}, \quad x \in (a_k, b_k), \tag{86}$$

$$D_y^*(x, 0^+, p) = D_y^*(x, 0^-, p) = -\frac{D_\infty - D^*}{p}, \quad x \in (a_k, b_k). \tag{87}$$

According to the above derivation method, the DSIF and electric displacement intensity factor of a_k and b_k are expressed as

$$\lim_{x \rightarrow a_k^-} \tau_{yz}(x, 0, p) = \frac{\tau_\infty H_1^*}{p R^*} \lim_{l_k \rightarrow -1^-} \frac{h_{1(k)}(-1)}{\sqrt{l_k^2 - 1}} + \frac{\tau_\infty H_2^*}{p R^*} \lim_{l_k \rightarrow -1^-} \frac{h_{2(k)}(-1)}{\sqrt{l_k^2 - 1}}, \tag{88a}$$

$$\lim_{x \rightarrow a_k^-} D_y(x, 0, p) = \frac{D_\infty H_3^*}{p R^*} \lim_{l_k \rightarrow -1^-} \frac{h_{1(k)}(-1)}{\sqrt{l_k^2 - 1}} + \frac{D_\infty H_4^*}{p R^*} \lim_{l_k \rightarrow -1^-} \frac{h_{2(k)}(-1)}{\sqrt{l_k^2 - 1}}, \tag{88b}$$

$$\lim_{x \rightarrow b_k^+} \tau_{yz}(x, 0, p) = \frac{\tau_\infty H_1^*}{p R^*} \lim_{l_k \rightarrow 1^+} \frac{-h_{1(k)}(1)}{\sqrt{l_k^2 - 1}} + \frac{\tau_\infty H_2^*}{p R^*} \lim_{l_k \rightarrow 1^+} \frac{-h_{2(k)}(1)}{\sqrt{l_k^2 - 1}}, \tag{88c}$$

$$\lim_{x \rightarrow b_k^+} D_y(x, 0, p) = \frac{D_\infty H_3^*}{p R^*} \lim_{l_k \rightarrow 1^+} \frac{-h_{1(k)}(1)}{\sqrt{l_k^2 - 1}} + \frac{D_\infty H_4^*}{p R^*} \lim_{l_k \rightarrow 1^+} \frac{-h_{2(k)}(1)}{\sqrt{l_k^2 - 1}}. \tag{88d}$$

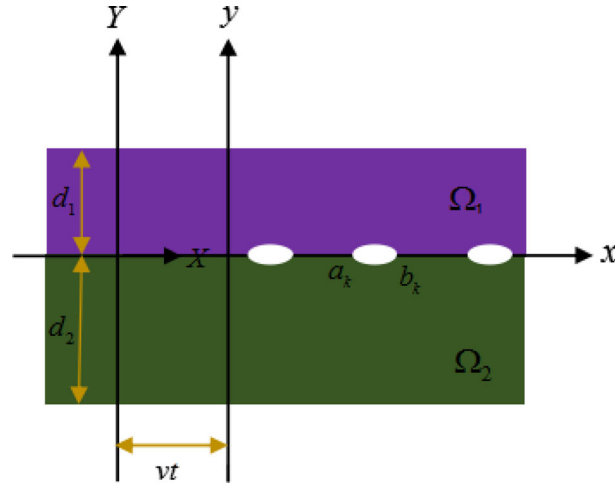


Fig. 1 Multiple interfacial propagating cracks between the piezoelectric thin film /substrate

4.1 Impermeable cracks (D-P boundary condition)

For impermeable cracks, the electrical displacement within the crack is negligible because the dielectric constant of the piezoelectric material is 3–4 orders of magnitude larger than that of air or vacuum. D^* in Eq. (85) satisfies the following condition [5]:

$$D^* = 0. \quad (89)$$

We have

$$K_{III}(a_k) = \tau_\infty \sqrt{\pi a_k} (Z_{1k}(t) + Z_{2k}(t)), \quad (90a)$$

$$K_{IV}(a_k) = D_\infty \sqrt{\pi a_k} (Z_{3k}(t) + Z_{4k}(t)), \quad (90b)$$

$$K_{III}(b_k) = -\tau_\infty \sqrt{\pi b_k} (Z_{5k}(t) + Z_{6k}(t)), \quad (90c)$$

$$K_{IV}(b_k) = -D_\infty \sqrt{\pi b_k} (Z_{7k}(t) + Z_{8k}(t)), \quad (90d)$$

where $Z_{1k}(t) = \frac{1}{2\pi i} \int_{B_r} \frac{H_1^*}{pR^*} h_{1(k)}(-1) e^{pt} dp$, $Z_{2k}(t) = \frac{1}{2\pi i} \int_{B_r} \frac{H_2^*}{pR^*} h_{2(k)}(-1) e^{pt} dp$, $Z_{3k}(t) = \frac{1}{2\pi i} \int_{B_r} \frac{H_3^*}{pR^*} h_{1(k)}(-1) e^{pt} dp$, $Z_{4k}(t) = \frac{1}{2\pi i} \int_{B_r} \frac{H_4^*}{pR^*} h_{2(k)}(-1) e^{pt} dp$, $Z_{5k}(t) = \frac{1}{2\pi i} \int_{B_r} \frac{H_1^*}{pR^*} h_{1(k)}(1) e^{pt} dp$, $Z_{6k}(t) = \frac{1}{2\pi i} \int_{B_r} \frac{H_2^*}{pR^*} h_{2(k)}(1) e^{pt} dp$, $Z_{7k}(t) = \frac{1}{2\pi i} \int_{B_r} \frac{H_3^*}{pR^*} h_{1(k)}(1) e^{pt} dp$, $Z_{8k}(t) = \frac{1}{2\pi i} \int_{B_r} \frac{H_4^*}{pR^*} h_{2(k)}(1) e^{pt} dp$.

According to Eqs. (90a–90d) and the virtual crack closure technique, we can obtain the energy release rate [33]

$$G(a_k) = \frac{\pi a_k}{4} (\varpi_1 K_{III}^2 + \varpi_2 K_{III} K_{IV} + \varpi_3 K_{IV}^2), \quad (91)$$

where $\varpi_1 = \frac{Z_{4k}(t)}{\Xi}$,

$$\varpi_2 = -\frac{Z_{3k}(t) + Z_{2k}(t)}{\Xi},$$

$$\varpi_3 = \frac{Z_{1k}(t)}{\Xi},$$

$$\Xi = \begin{vmatrix} Z_{1k}(t) & Z_{2k}(t) \\ Z_{3k}(t) & Z_{4k}(t) \end{vmatrix}.$$

One can see

$$K_{III}(a_k) = \tau_\infty \sqrt{\pi a_k} Y_{1k}(t), \quad (92a)$$

$$K_{IV}(a_k) = D_\infty \sqrt{\pi a_k} Y_{2k}(t), \quad (92b)$$

$$K_{III}(b_k) = -\tau_\infty \sqrt{\pi b_k} Y_{3k}(t), \quad (92c)$$

$$K_{IV}(a_k) = -D_\infty \sqrt{\pi b_k} Y_{4k}(t), \quad (92c)$$

where

$$\begin{aligned} Y_{1k}(t) &= \frac{1}{2\pi i} \int_{Br} \left[\frac{H_1^*}{pR^*} h_{1(k)}(-1) + \frac{H_2^*}{pR^*} h_{2(k)}(-1) \right] e^{pt} dp, \\ Y_{2k}(t) &= \frac{1}{2\pi i} \int_{Br} \left[\frac{H_3^*}{pR^*} h_{1(k)}(-1) + \frac{H_4^*}{pR^*} h_{2(k)}(-1) \right] e^{pt} dp, \\ Y_{3k}(t) &= \frac{1}{2\pi i} \int_{Br} \left[\frac{H_1^*}{pR^*} h_{1(k)}(1) + \frac{H_2^*}{pR^*} h_{2(k)}(1) \right] e^{pt} dp, \\ Y_{4k}(t) &= \frac{1}{2\pi i} \int_{Br} \left[\frac{H_3^*}{pR^*} h_{1(k)}(1) + \frac{H_4^*}{pR^*} h_{2(k)}(1) \right] e^{pt} dp. \end{aligned}$$

4.2 Permeable cracks

The joint degree of electromechanical load can be expressed as

$$e_{15} D_\infty / \varepsilon_{11} \tau_\infty = \lambda, \quad (93)$$

where λ is a parameter.

For permeable cracks, the electric potential on the upper and lower surfaces of the crack is continuous:

$$h_{\varphi(k)}(x) = 0. \quad (94)$$

By applying the inverse Laplace transform, the DSIF and dynamic electric displacement intensity factor are written as

$$K_{III}(a_k) = \sqrt{2\pi(a_k - x)}_{x \rightarrow a_k - 0} \tau_{yz}(x, 0, t) = \sqrt{\pi a_k} \tau_\infty S_{1k}(t), \quad (95)$$

$$K_{IV}(a_k) = \sqrt{2\pi(a_k - x)}_{x \rightarrow a_k - 0} D_y(x, 0, t) = \frac{\lambda \varepsilon_{11}}{e_{15}} \sqrt{\pi a_k} \tau_\infty S_{2k}(t), \quad (96)$$

$$K_{III}(b_k) = \sqrt{2\pi(x - b_k)}_{x \rightarrow b_k + 0} \tau_{yz}(x, 0, t) = \sqrt{\pi b_k} \tau_\infty S_{3k}(t), \quad (97)$$

$$K_{IV}(b_k) = \sqrt{2\pi(x - b_k)}_{x \rightarrow b_k + 0} D_y(x, 0, t) = \frac{\lambda \varepsilon_{11}}{e_{15}} \sqrt{\pi b_k} \tau_\infty S_{4k}(t), \quad (98)$$

where $S_{1k}(t) = \frac{1}{2\pi i} \int_{Br} \frac{H_1^*}{pR^*} h_{1(k)}(-1) e^{pt} dp$, $S_{2k}(t) = \frac{1}{2\pi i} \int_{Br} \frac{H_3^*}{pR^*} h_{1(k)}(-1) e^{pt} dp$,

$S_{3k}(t) = \frac{1}{2\pi i} \int_{Br} \frac{H_1^*}{pR^*} h_{1(k)}(1) e^{pt} dp$, $S_{4k}(t) = \frac{1}{2\pi i} \int_{Br} \frac{H_3^*}{pR^*} h_{1(k)}(1) e^{pt} dp$.

From the previous results, we find that the DSIF and dynamic electrical-displacement intensity factors are related to the applied impact stress and material properties. The singularity of the electrical displacement is derived from the electromechanical coupling effect. This conclusion is consistent with that in [31].

5 Numerical examples

This section consists of three parts. In the first part, numerical validation is performed with previous work to verify the correctness of the theoretical derivation. In the second part, numerical examples of double- and triple-interface cracks are presented. The influence of material constants, v and t/t_0 are discussed. Our research yields some new conclusions. The crack length is $2a$, and the thickness of the single material is denoted by d . The value of t_0 is $1 \mu\text{s}$, and the unit of t/t_0 is ms. The electromechanical coupling coefficient is represented by k . In the third part, the influence of τ_∞ and D_∞ on the dynamic energy release rate are discussed.

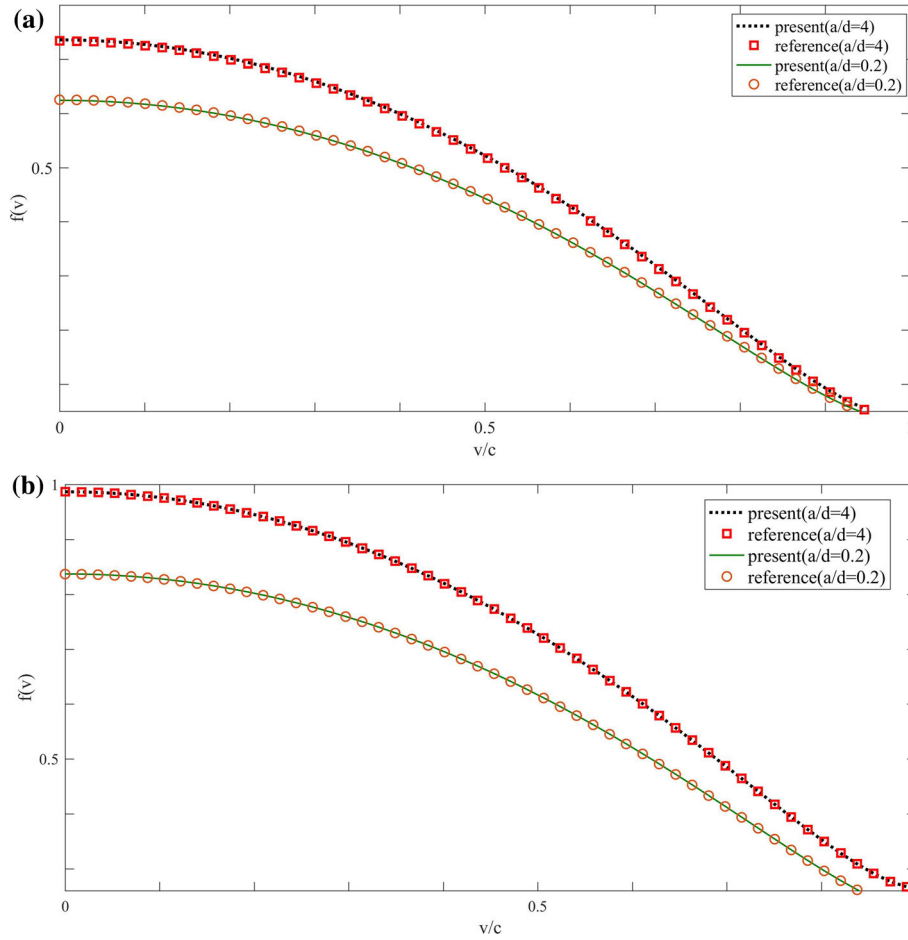


Fig. 2 The nondimensional function $f(v)$ versus v/c for the following piezoelectric thin film/substrate materials: **a** PZT-4/PZT-5H and **b** BaTiO₃/PZT65/35

5.1 Numerical validation with the previous results

Some numerical validations are performed with previous results [17]. We choose PZT-4/PZT-5H and BaTiO₃/PZT65/35 for our research. The corresponding analysis diagram is presented in Fig. 2. We show the change in the nondimensional function $f(v)$ with two different piezoelectric film thicknesses. Each is plotted against v/c for two different piezoelectric thin film/substrate materials. The larger the ratio of the crack size to material thickness is, the more significant the nondimensional function $f(v)$. In other words, the thinner the film is, the higher the nondimensional function $f(v)$. We also find that the smaller the electromechanical coupling coefficient is, the larger is nondimensional function $f(v)$. This result is consistent with the result in Ref. [17].

Figure 3a-d show the change in the nondimensional function $f(v)$ at five different piezoelectric film thicknesses. Each is plotted against v/c for four different piezoelectric thin film/substrate materials. When the film thickness is smaller, the nondimensional function $f(v)$ increases. The nondimensional function $f(v)$ is controlled by the piezoelectric film thickness, i.e., the thinner the film thickness is, the greater its influence on the nondimensional DSIF. In addition, the variation law of crack growth is consistent with that in Refs. [14] and [15].

Figure 4a shows the nondimensional function $f(v)$ of a PVDF thin film/PZT-5H substrate and the ratio of the piezoelectric film thickness to crack length. Figure 4b shows the nondimensional function $f(v)$ of a PVDF thin film/PZT-4 substrate and the ratio of the piezoelectric film thickness to crack length. Under four different conditions, the normalized stress intensity factor increases with the decrease in $d_1/2a$. When the substrate thickness is constant, the thinner the film is, the more pronounced the effect. By comparing the

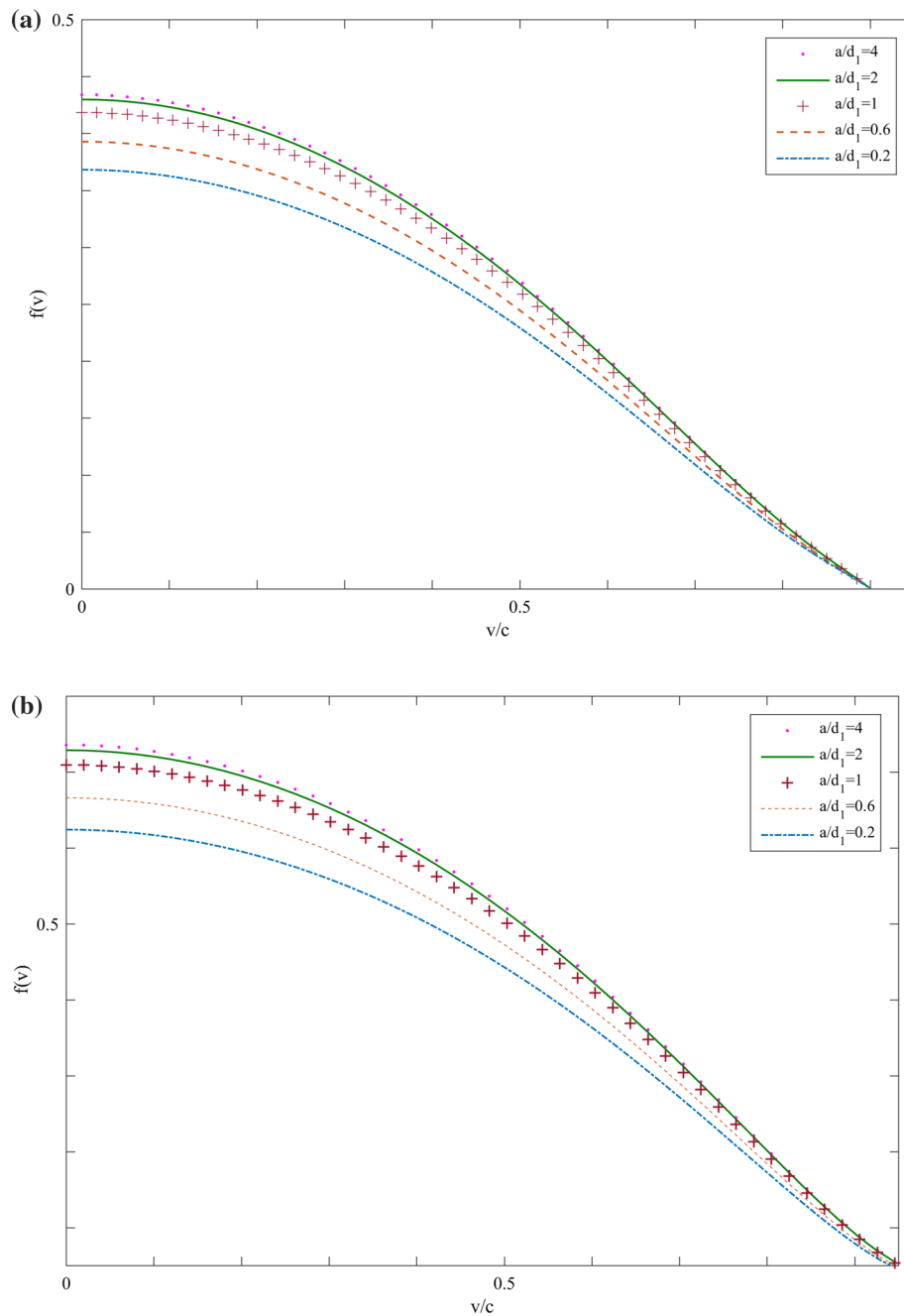


Fig. 3 The $f(v)$ versus the nondimensional velocity v/c for the following piezoelectric thin film/substrate materials: **a** PZT-4/PZT-5H; **b** PZT-4/BaTiO₃; **c** PZT65/35/PZT-5H; **d** BaTiO₃/PZT65/35

two figures, we can observe that when the ratio of the film thickness to the substrate is constant, the influence of a smaller electromechanical coupling coefficient on $f(v)$ becomes more apparent.

Figure 5a shows the nondimensional function $f(v)$ of a PVDF thin film/PZT-4 substrate and the ratio of t to t_0 . Figure 5b shows the nondimensional function $f(v)$ of a PVDF thin film/PZT – 5H substrate and the ratio of t to t_0 . We can observe that $f(v)$ increases as the dimensionless time increases. We can clearly see that when the film thickness is constant, the thicker the substrate is, the lesser its influence on the nondimensional function $f(v)$. The dynamic nondimensional stress intensity factor reaches a peak and then tends to static values.

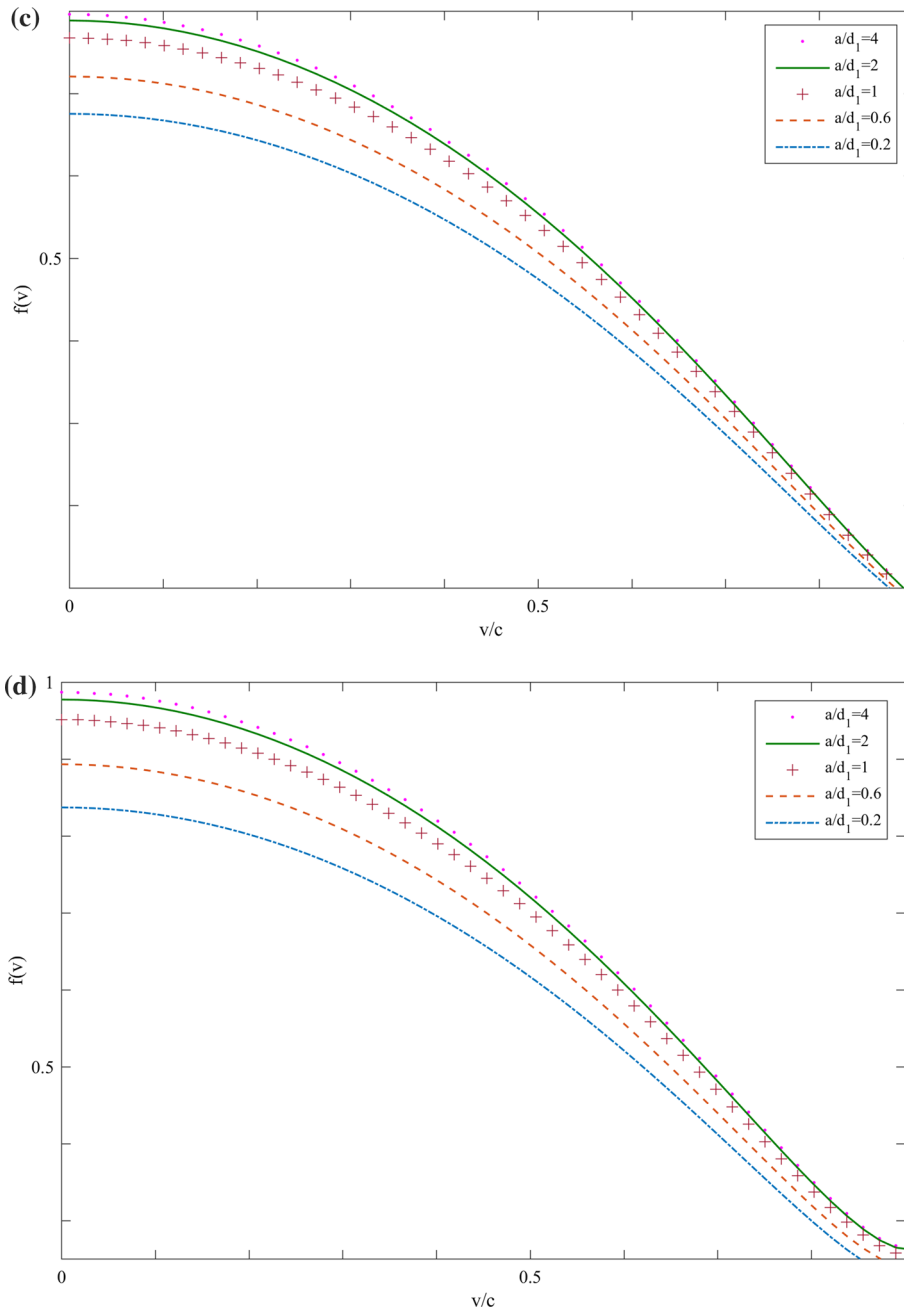


Fig. 3 continued

5.2 The double- and triple-interface cracks

We now focus on the multiple-fracture solution: On this basis, the interaction behavior of interfacial cracks under impact loading is investigated in detail. Figures 6 and 7 show the numerical results.

Under dynamic loading, $f(v)$ of the piezoelectric thin film/substrate with double interface cracks is obviously different from that of a single crack. The variations in the nondimensional DSIF against $d_1/(2a)$ as a function of crack distance $d_1/(2a)$ are computed.

In the case of multiple cracks, according to their mutual effects, the nondimensional DSIF inside the crack tip is more significant than that outside the crack tip, regardless of the number of cracks. Figure 6a shows that when the film thickness is constant, the larger the crack size is, the larger its influence on the nondimensional

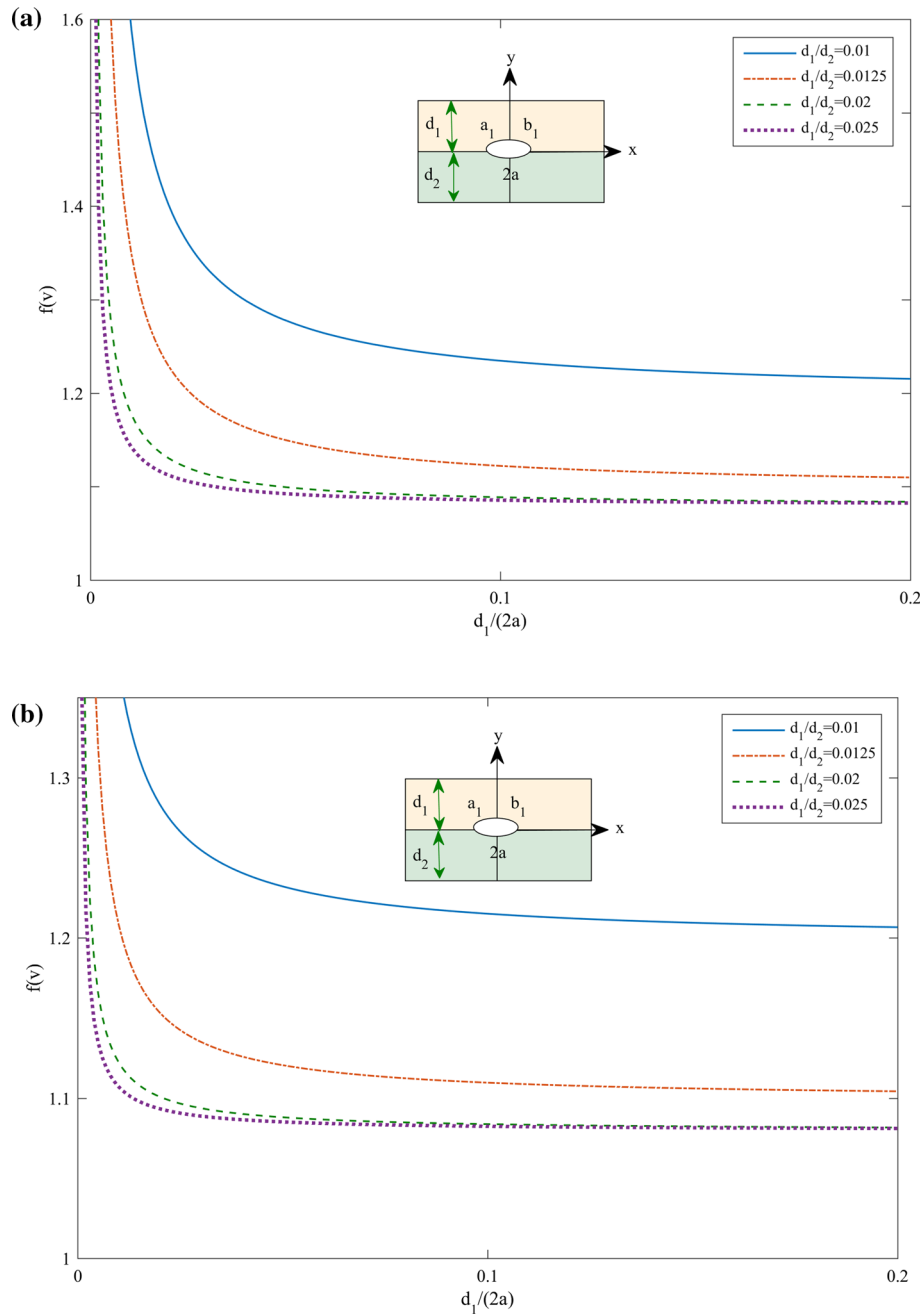


Fig. 4 Variations of $f(v)$ versus $d_1/(2a)$ for different piezoelectric thin film/substrate materials PVDF thin film/PZT-5H substrate and PVDF thin film/PZT-4 substrate

function $f(v)$. We can clearly see that when the film thickness is constant, the thicker the substrate is, the lesser its influence on the nondimensional function $f(v)$ in Fig. 7. Figure 6b shows that when the substrate thickness is constant, the film thickness is small, and the change in the nondimensional stress intensity factor is large, which indicates that under appropriate circumstances, a thinner film thickness is more conducive to safe design.

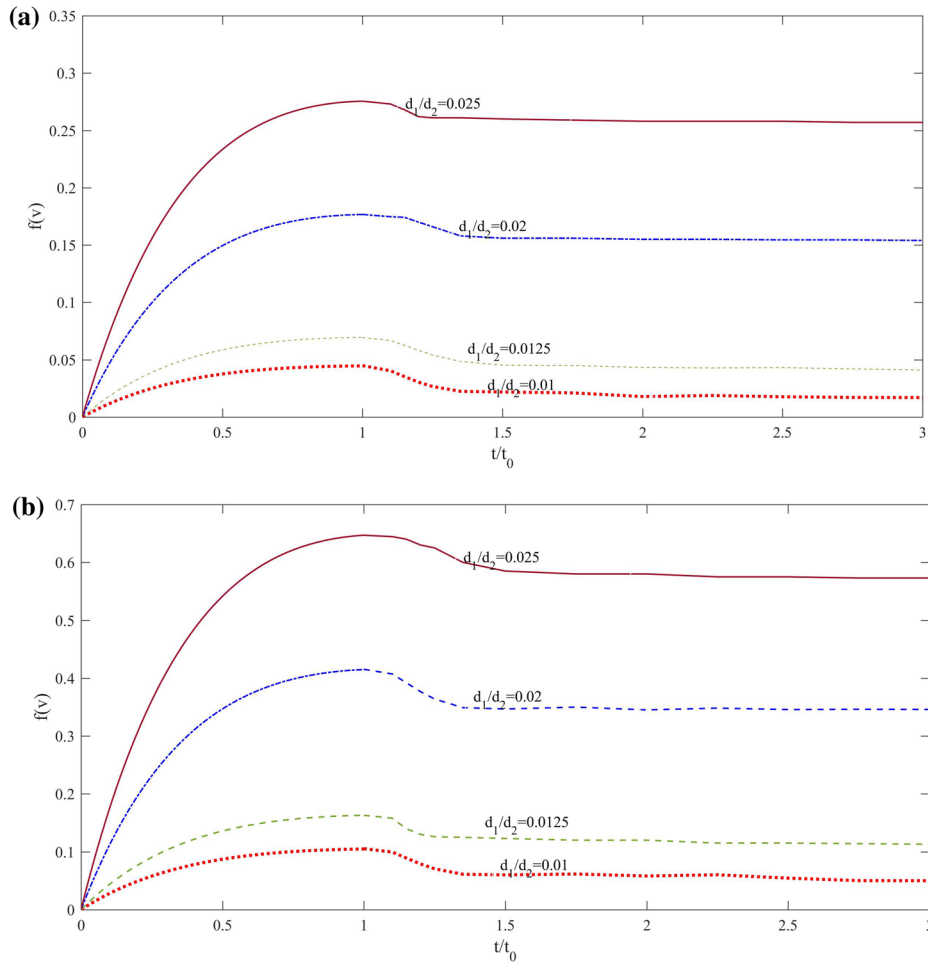


Fig. 5 Variations in $f(v)$ versus t/t_0 for different piezoelectric thin film/substrate materials **a** PVDF thin film/PZT – 4 substrate and **b** PVDF thin film/PZT – 5H substrate

5.3 Impermeable and permeable cracks

According to Eq. (91), the dynamic nondimensional energy-release rate can be expressed G/G_r (G_r is the dynamic energy-release rate for a stationary crack). According to Eq. (95), the nondimensional DSIF can be defined as F_0 .

Figure 8 shows the effect of stress on the nondimensional energy-release rate at different values ($PZT - 5$ thin film/ $PZT - 5$ substrate). Figure 8 shows that when τ_∞ increases from zero, G/G_r always increases. However, when τ_∞ decreases from zero, G/G_r will first decrease and then increase. The stress loading pushes or interferes with the crack growth.

Figure 9 shows the effects of the electrical displacement and stress on the nondimensional energy-release rate at different values. As a result, their effects on the energy-release rate take the form of a parabola at different values. Figure 9 shows that when D_∞ decreases from zero, G/G_r decreases. However, when D_∞ increases ($a > 0$), G/G_r first increases and then decreases. The result suggests that when the electrical displacement is negative, crack growth can be hindered. However, positive electric-displacement loads can promote or hinder crack growth. This is discussed by Pak [5].

To better investigate dynamic crack propagation under mechanical and electrical impacts. Figure 10 shows the nondimensional dynamic intensity factors under different values of λ . As shown, when $ct/(2a)$ proceeds, F_0 first increases, peaks and finally flattens, which is similar to the result presented by Wang [32].

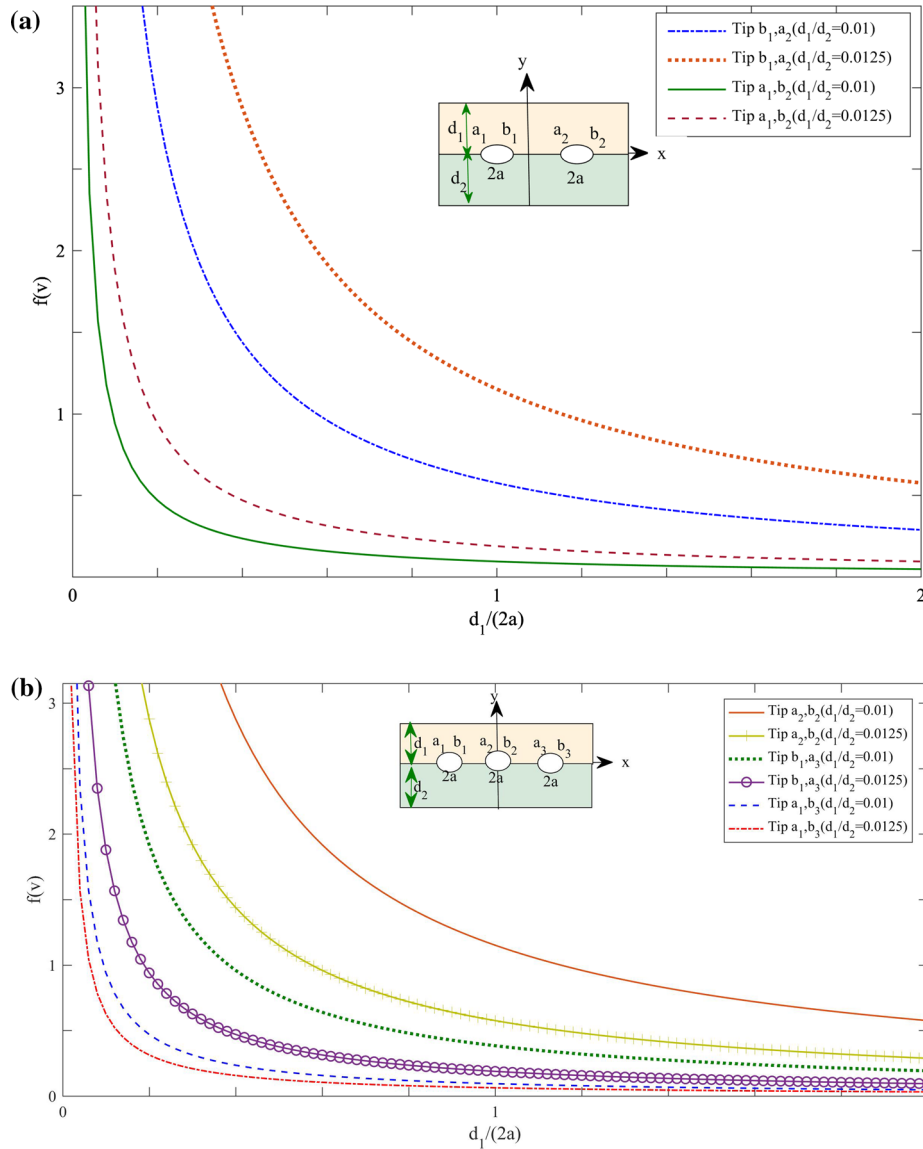


Fig. 6 Variations of $f(v)$ with versus for different piezoelectric thin film/substrate materials PZT-4 thin film/PZT-4 substrate and PVDF thin film/PZT-4 substrate

6 Conclusions

The dynamic fracture characteristics of mode-III cracks are investigated. The theoretical solution to this problem is described using the integral-transform method (Laplace and Fourier transforms) and the Chebyshev point method. By analysis, the following conclusions are presented: (1) When the film thickness is thinner, the nondimensional functions increase. The nondimensional functions are controlled by the piezoelectric film thickness. (2) The nondimensional DSIF increases with decreasing $d_1/(2a)$. (3) When the thickness of the film is constant, the thinner the substrate is, the more apparent the effect. When the ratio of the film thickness to substrate remains constant, the influence of the smaller electromechanical coupling coefficient on the nondimensional DSIF becomes more evident. (4) The nondimensional DSIF increases as the dimensionless time increases. We can observe that when the thickness of the substrate is constant, the thinner the film is, the more significant the influence on the nondimensional functions. (5) The nondimensional DSIF of multiple cracks is clearly more significant than that of a single crack when the film thickness is the same. (6) The nondimensional DSIF of the crack tip inside is more significant than that outside the crack tip of the dimensionless DSIF, irrespective of the number of cracks. (7) Stress loading can promote or prevent crack

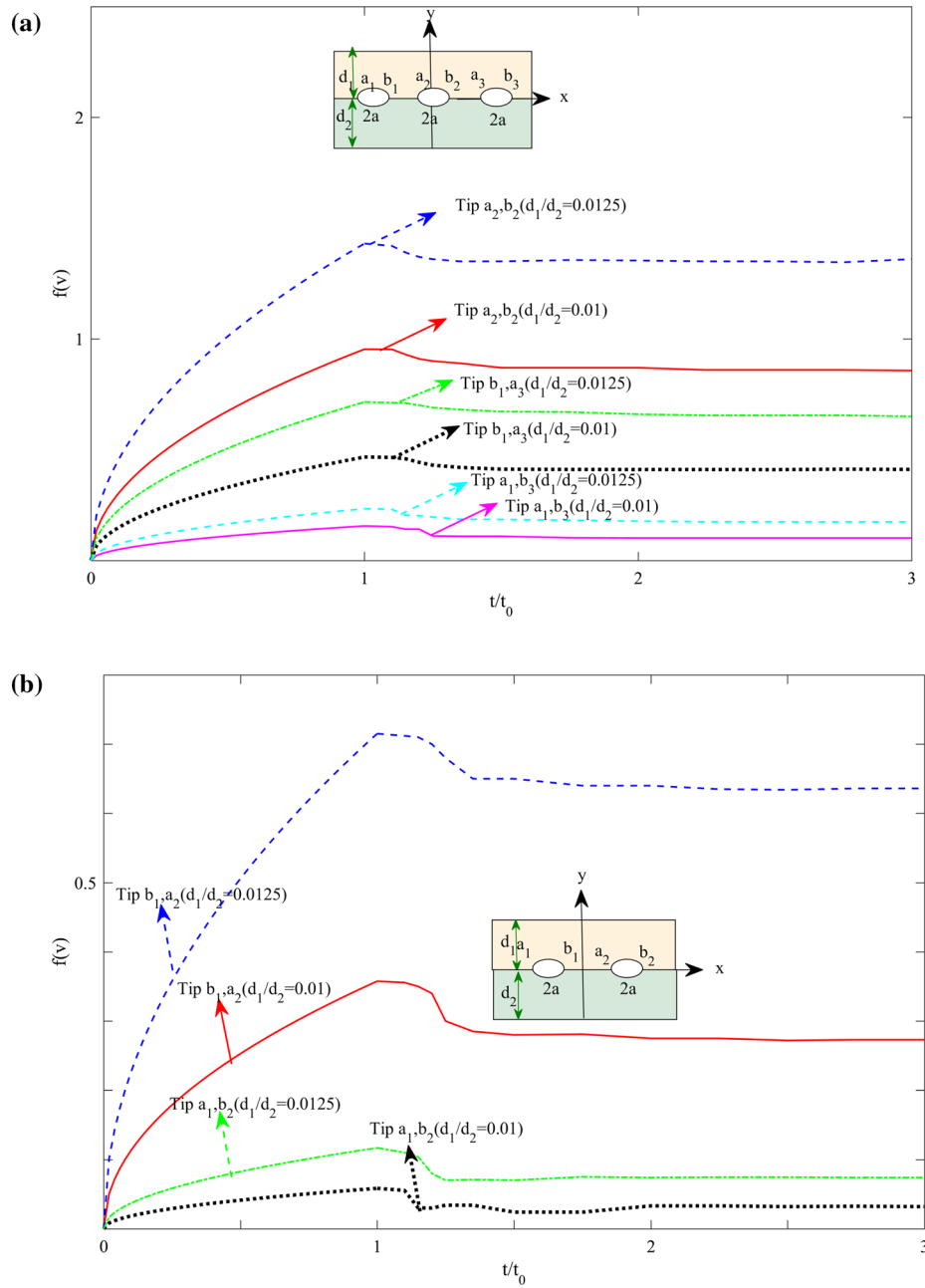


Fig. 7 Variations of $f(v)$ with versus t/t_0 for different piezoelectric thin-film/substrate materials PZT-4 thin film/PZT-4 substrate and PVDF thin film/PZT-4 substrate

propagation. (8) Negative electrical displacement loads always prevent crack propagation, whereas positive electric-displacement loads can promote or prevent crack propagation.

It is believed that the stress intensity factor is related to crack size, component geometry, and loading. According to the analysis in the current work, the larger crack size is, the more significant the nondimensional DSIF is. The smaller the electromechanical coupling coefficient is, the larger the nondimensional DSIF is. The thinner the film thickness is, the larger the nondimensional DSIF is. The larger the nondimensional DSIF is

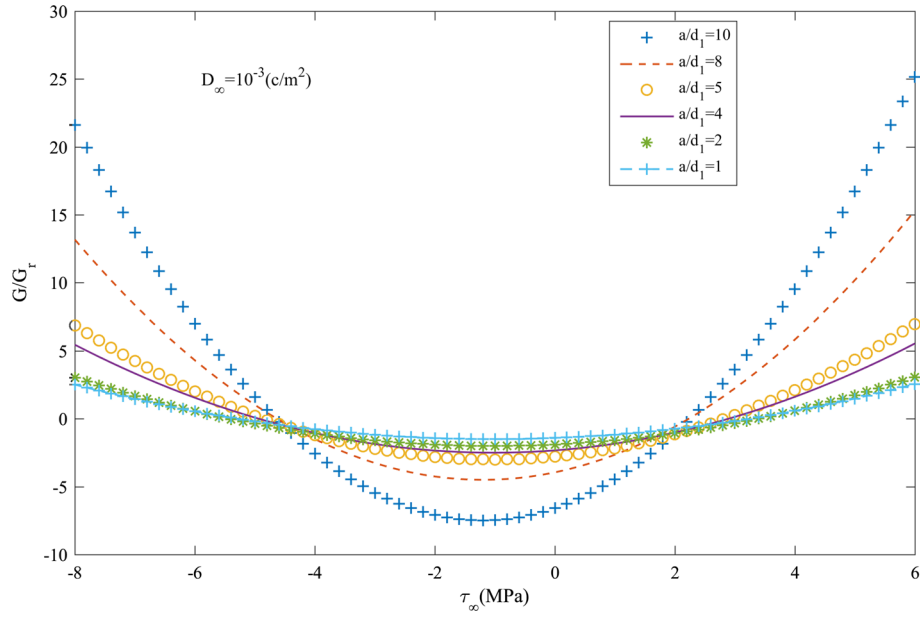


Fig. 8 Influence of stress on the energy-release rate at different values a/d_1

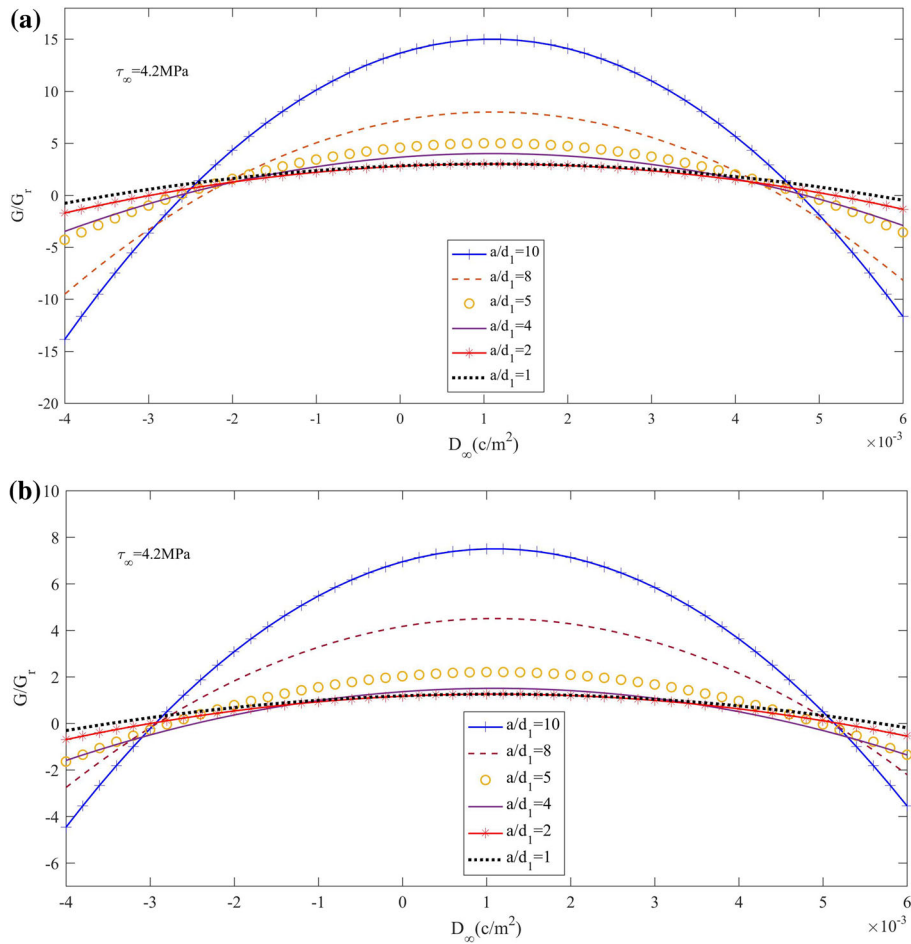


Fig. 9 Influence of electric displacement on energy release rate at different values a/d_1 **a:** PZT-5 thin film/PZT-5 substrate; **b:** PZT-4 thin film/PZT-4 substrate

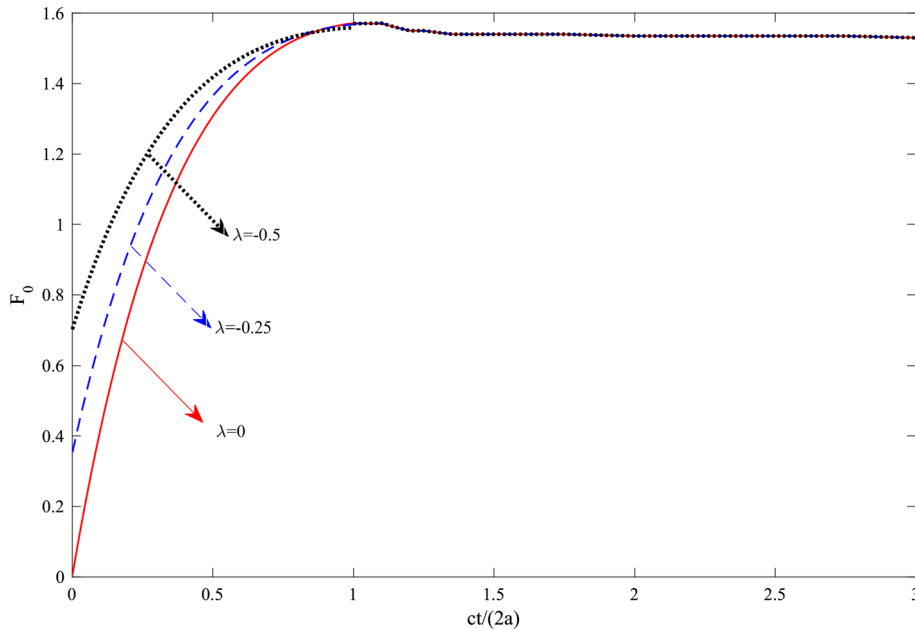


Fig. 10 The variation in the nondimensional DSIF under different values λ

the crack tip is, the more pronounced the stress concentration at the crack tip is. If the nondimensional DSIF exceeds the critical value, then the crack will expand and fracture. Therefore, under appropriate conditions, the thinner the film is, the safer is the structure design.

Acknowledgements This study was supported by the National Natural Science Foundation of China (11972019), Shanxi Provincial Key Research and Development Project (202102090301027), and Shanxi Postgraduate Innovation Project (2022Y668).

Data availability All the numerical calculated data used to support the findings of this study can be obtained by calculating the equations in the paper, and piezoelectric material parameters are taken from references [14, 15] and [34–36].

Declarations

Conflict of interest The authors declare that there are no conflicts of interest regarding the publication of this paper.

Appendix

$$\begin{aligned}
 R_1 &= \left[-e_{15}^{(1)} \frac{\varepsilon_{11}^{(2)}}{\varepsilon_{11}^{(1)}} (1 - e^{-2|\zeta|d_2}) + e_{15}^{(2)} \frac{\varepsilon_{11}^{(2)}}{\varepsilon_{11}^{(1)}} (1 - e^{-2|\zeta|d_2}) \right] \left[-\frac{e_{15}^{(2)}}{\varepsilon_{11}^{(2)}} (1 + e^{-2\alpha_2 d_2}) \right] e^{-2\alpha_1 d_1} \\
 &\quad - \frac{\alpha_2}{|\zeta|} \left\{ c_{44}^{(2)} \left(1 + \frac{e_{15}^{(2)} e_{15}^{(2)}}{\varepsilon_{11}^{(2)}} \right) (1 - e^{-2\alpha_2 d_2}) \left[-\frac{\varepsilon_{11}^{(2)} (1 - e^{-2|\zeta|d_2}) (1 + e^{-2|\zeta|d_1})}{\varepsilon_{11}^{(1)} (1 - e^{-2|\zeta|d_1})} - (1 + e^{-2|\zeta|d_2}) \right] \right\} e^{-2\alpha_1 d_1} \\
 R_2 &= \left[e_{15}^{(1)} \frac{\varepsilon_{11}^{(2)}}{\varepsilon_{11}^{(1)}} (1 - e^{-2|\zeta|d_2}) - e_{15}^{(2)} (1 - e^{-2|\zeta|d_2}) \right] (-1 - e^{-2\alpha_2 d_2}) e^{-2\alpha_1 d_1} \\
 &= (1 - e^{-2|\zeta|d_2}) (1 + e^{-2\alpha_2 d_2}) \left(\frac{e_{15}^{(2)} \varepsilon_{11}^{(1)} - e_{15}^{(1)} \varepsilon_{11}^{(2)}}{\varepsilon_{11}^{(1)}} \right) e^{-2\alpha_1 d_1} \\
 R_3 &= \left[(1 - e^{-2|\zeta|d_2}) \frac{e_{15}^{(2)} \varepsilon_{11}^{(1)} - e_{15}^{(1)} \varepsilon_{11}^{(2)}}{\varepsilon_{11}^{(1)}} \right] \left[\frac{e_{15}^{(2)}}{\varepsilon_{11}^{(2)}} (1 + e^{-2\alpha_2 d_2}) \right]
 \end{aligned}$$

$$\begin{aligned}
& -\frac{\alpha_2}{|\zeta|} \left\{ c_{44}^{(2)} \left(1 + \frac{e_{15}^{(2)} e_{15}^{(2)}}{\varepsilon_{11}^{(2)}} \right) (1 - e^{-2\alpha_2 d_2}) \left[-\frac{\varepsilon_{11}^{(2)} (1 - e^{-2|\zeta| d_2}) (1 + e^{-2|\zeta| d_1})}{\varepsilon_{11}^{(1)} (1 - e^{-2|\zeta| d_1})} - (1 + e^{-2|\zeta| d_2}) \right] \right\} \\
R_4 &= (1 - e^{-2|\zeta| d_2}) (1 + e^{-2\alpha_2 d_2}) \left(\frac{e_{15}^{(2)} \varepsilon_{11}^{(1)} - e_{15}^{(1)} \varepsilon_{11}^{(2)}}{\varepsilon_{11}^{(1)}} \right) \\
R_5 &= -\frac{\alpha_1}{|\zeta|} \left[(1 + e^{-2|\zeta| d_2}) + \frac{\varepsilon_{11}^{(2)} (1 - e^{-2|\zeta| d_2}) (1 + e^{-2|\zeta| d_1})}{\varepsilon_{11}^{(1)} (1 - e^{-2|\zeta| d_1})} \right] c_{44}^{(1)} \left(1 + \frac{e_{15}^{(1)} e_{15}^{(1)}}{\varepsilon_{11}^{(1)}} \right) (1 - e^{-2\alpha_1 d_1}) \\
& + \frac{e_{15}^{(1)}}{\varepsilon_{11}^{(1)}} (1 + e^{-2\alpha_1 d_1}) \left[\frac{e_{15}^{(1)} \varepsilon_{11}^{(2)}}{\varepsilon_{11}^{(1)}} (1 - e^{-2|\zeta| d_2}) - e_{15}^{(2)} (1 - e^{-2|\zeta| d_2}) \right] \\
R_6 &= (1 + e^{-2\alpha_1 d_1}) (1 - e^{-2|\zeta| d_2}) \left(e_{15}^{(2)} - \frac{e_{15}^{(1)} \varepsilon_{11}^{(2)}}{\varepsilon_{11}^{(1)}} \right) \\
R_7 &= -\frac{\alpha_1}{|\zeta|} (1 - e^{-2\alpha_1 d_1}) e^{-2\alpha_2 d_2} c_{44}^{(1)} \left(1 + \frac{e_{15}^{(1)} e_{15}^{(1)}}{\varepsilon_{11}^{(1)}} \right) \left[(1 + e^{-2|\zeta| d_2}) + \frac{\varepsilon_{11}^{(2)} (1 - e^{-2|\zeta| d_2}) (1 + e^{-2|\zeta| d_1})}{\varepsilon_{11}^{(1)} (1 - e^{-2|\zeta| d_1})} \right] \\
& + (1 - e^{-2|\zeta| d_2}) (1 + e^{-2\alpha_1 d_1}) e^{-2\alpha_2 d_2} \frac{e_{15}^{(1)} (e_{15}^{(1)} \varepsilon_{11}^{(2)} - e_{15}^{(2)} \varepsilon_{11}^{(1)})}{\varepsilon_{11}^{(1)} \varepsilon_{11}^{(1)}} \\
R_8 &= (1 + e^{-2\alpha_1 d_1}) (1 - e^{-2|\zeta| d_2}) e^{-2\alpha_2 d_2} \frac{e_{15}^{(2)} \varepsilon_{11}^{(1)} - e_{15}^{(1)} \varepsilon_{11}^{(2)}}{\varepsilon_{11}^{(1)}} \\
R_9 &= -\frac{\varepsilon_{11}^{(2)}}{\varepsilon_{11}^{(1)}} e^{-2|\zeta| d_1} \frac{1 - e^{-2|\zeta| d_2}}{1 - e^{-2|\zeta| d_1}} \left[\frac{\alpha_2}{|\zeta|} c_{44}^{(2)} \left(1 + \frac{e_{15}^{(2)} e_{15}^{(2)}}{\varepsilon_{11}^{(2)}} \right) \frac{e_{15}^{(1)}}{\varepsilon_{11}^{(1)}} (1 - e^{-2\alpha_2 d_2}) (1 + e^{-2\alpha_1 d_1}) \right. \\
& \left. + \frac{\alpha_1}{|\zeta|} c_{44}^{(1)} \left(1 + \frac{e_{15}^{(1)} e_{15}^{(1)}}{\varepsilon_{11}^{(1)}} \right) \frac{e_{15}^{(2)}}{\varepsilon_{11}^{(2)}} (1 - e^{-2\alpha_1 d_1}) (1 + e^{-2\alpha_2 d_2}) \right] \\
R_{10} &= -\left[\frac{\alpha_2}{|\zeta|} c_{44}^{(2)} \left(1 + \frac{e_{15}^{(2)} e_{15}^{(2)}}{\varepsilon_{11}^{(2)}} \right) (1 - e^{-2\alpha_2 d_2}) (1 + e^{-2\alpha_1 d_1}) \right. \\
& \left. + \frac{\alpha_1}{|\zeta|} c_{44}^{(1)} \left(1 + \frac{e_{15}^{(1)} e_{15}^{(1)}}{\varepsilon_{11}^{(1)}} \right) (1 - e^{-2\alpha_1 d_1}) (1 + e^{-2\alpha_2 d_2}) \right] \frac{\varepsilon_{11}^{(2)}}{\varepsilon_{11}^{(1)}} e^{-2|\zeta| d_1} \frac{1 - e^{-2|\zeta| d_2}}{1 - e^{-2|\zeta| d_1}} \\
R_{11} &= -\frac{\varepsilon_{11}^{(2)}}{\varepsilon_{11}^{(1)}} \frac{1 - e^{-2|\zeta| d_2}}{1 - e^{-2|\zeta| d_1}} \left[\frac{\alpha_2}{|\zeta|} c_{44}^{(2)} \left(1 + \frac{e_{15}^{(2)} e_{15}^{(2)}}{\varepsilon_{11}^{(2)}} \right) \frac{e_{15}^{(1)}}{\varepsilon_{11}^{(1)}} (1 - e^{-2\alpha_2 d_2}) (1 + e^{-2\alpha_1 d_1}) \right. \\
& \left. + \frac{\alpha_1}{|\zeta|} c_{44}^{(1)} \left(1 + \frac{e_{15}^{(1)} e_{15}^{(1)}}{\varepsilon_{11}^{(1)}} \right) \frac{e_{15}^{(2)}}{\varepsilon_{11}^{(2)}} (1 - e^{-2\alpha_1 d_1}) (1 + e^{-2\alpha_2 d_2}) \right] \\
R_{12} &= -\frac{\varepsilon_{11}^{(2)}}{\varepsilon_{11}^{(1)}} \frac{1 - e^{-2|\zeta| d_2}}{1 - e^{-2|\zeta| d_1}} \left[\frac{\alpha_2}{|\zeta|} c_{44}^{(2)} \left(1 + \frac{e_{15}^{(2)} e_{15}^{(2)}}{\varepsilon_{11}^{(2)}} \right) (1 - e^{-2\alpha_2 d_2}) (1 + e^{-2\alpha_1 d_1}) \right. \\
& \left. + \frac{\alpha_1}{|\zeta|} c_{44}^{(1)} \left(1 + \frac{e_{15}^{(1)} e_{15}^{(1)}}{\varepsilon_{11}^{(1)}} \right) (1 - e^{-2\alpha_1 d_1}) (1 + e^{-2\alpha_2 d_2}) \right] \\
R_{13} &= \frac{\alpha_2}{|\zeta|} c_{44}^{(2)} \left(1 + \frac{e_{15}^{(2)} e_{15}^{(2)}}{\varepsilon_{11}^{(2)}} \right) \frac{e_{15}^{(1)}}{\varepsilon_{11}^{(1)}} (1 - e^{-2\alpha_2 d_2}) (1 + e^{-2\alpha_1 d_1}) \\
& + \frac{\alpha_1}{|\zeta|} c_{44}^{(1)} \left(1 + \frac{e_{15}^{(1)} e_{15}^{(1)}}{\varepsilon_{11}^{(1)}} \right) \frac{e_{15}^{(2)}}{\varepsilon_{11}^{(2)}} (1 - e^{-2\alpha_1 d_1}) (1 + e^{-2\alpha_2 d_2}) \\
R_{14} &= \frac{\alpha_2}{|\zeta|} c_{44}^{(2)} \left(1 + \frac{e_{15}^{(2)} e_{15}^{(2)}}{\varepsilon_{11}^{(2)}} \right) (1 - e^{-2\alpha_2 d_2}) (1 + e^{-2\alpha_1 d_1}) \\
& + \frac{\alpha_1}{|\zeta|} c_{44}^{(1)} \left(1 + \frac{e_{15}^{(1)} e_{15}^{(1)}}{\varepsilon_{11}^{(1)}} \right) (1 - e^{-2\alpha_1 d_1}) (1 + e^{-2\alpha_2 d_2})
\end{aligned}$$

$$\begin{aligned}
R_{15} &= e^{-2|\zeta|d_2} \left[\frac{\alpha_2}{|\zeta|} c_{44}^{(2)} \left(1 + \frac{e_{15}^{(2)} e_{15}^{(2)}}{\varepsilon_{11}^{(2)}} \right) \frac{e_{15}^{(1)}}{\varepsilon_{11}^{(1)}} (1 - e^{-2\alpha_2 d_2})(1 + e^{-2\alpha_1 d_1}) \right. \\
&\quad \left. + \frac{\alpha_1}{|\zeta|} c_{44}^{(1)} \left(1 + \frac{e_{15}^{(1)} e_{15}^{(1)}}{\varepsilon_{11}^{(1)}} \right) \frac{e_{15}^{(2)}}{\varepsilon_{11}^{(2)}} (1 - e^{-2\alpha_1 d_1})(1 + e^{-2\alpha_2 d_2}) \right] \\
R_{16} &= e^{-2|\zeta|d_2} \left[\frac{\alpha_2}{|\zeta|} c_{44}^{(2)} \left(1 + \frac{e_{15}^{(2)} e_{15}^{(2)}}{\varepsilon_{11}^{(2)}} \right) (1 - e^{-2\alpha_2 d_2})(1 + e^{-2\alpha_1 d_1}) \right. \\
&\quad \left. + \frac{\alpha_1}{|\zeta|} c_{44}^{(1)} \left(1 + \frac{e_{15}^{(1)} e_{15}^{(1)}}{\varepsilon_{11}^{(1)}} \right) (1 - e^{-2\alpha_1 d_1})(1 + e^{-2\alpha_2 d_2}) \right] \\
R &= \left[e_{15}^{(2)} (1 - e^{-2|\zeta|d_2}) - e_{15}^{(1)} \frac{\varepsilon_{11}^{(2)}}{\varepsilon_{11}^{(1)}} (1 - e^{-2|\zeta|d_2}) \right] \left(\frac{e_{15}^{(1)}}{\varepsilon_{11}^{(1)}} - \frac{e_{15}^{(2)}}{\varepsilon_{11}^{(2)}} \right) (1 + e^{-2\alpha_1 d_1})(1 + e^{-2\alpha_2 d_2}) \\
&\quad + \left[(1 + e^{-2|\zeta|d_2}) + \frac{\varepsilon_{11}^{(2)} (1 - e^{-2|\zeta|d_2})(1 + e^{-2|\zeta|d_1})}{\varepsilon_{11}^{(1)} (1 - e^{-2|\zeta|d_1})} \right] \left[\frac{\alpha_2}{|\zeta|} c_{44}^{(2)} \left(1 + \frac{e_{15}^{(2)} e_{15}^{(2)}}{\varepsilon_{11}^{(2)}} \right) (1 - e^{-2\alpha_2 d_2})(1 + e^{-2\alpha_1 d_1}) \right. \\
&\quad \left. + \frac{\alpha_1}{|\zeta|} c_{44}^{(1)} \left(1 + \frac{e_{15}^{(1)} e_{15}^{(1)}}{\varepsilon_{11}^{(1)}} \right) (1 - e^{-2\alpha_1 d_1})(1 + e^{-2\alpha_2 d_2}) \right]
\end{aligned}$$

References

- Shindo, Y., Tanaka, K., Narita, F.: Singular stress and electric fields of a piezoelectric ceramic strip with a finite crack under longitudinal shear. *Acta Mech.* **120**, 31–45 (1997)
- Deeg W.F.J.: The analysis of dislocation, crack, and inclusion problems in piezoelectric solids. Ph. D. Thesis. Stanford University (1980).
- Sosa, H.A., Pak, Y.E.: Three-dimensional eigenfunction analysis of a crack in a piezoelectric material. *Int. J. Solids Struct.* **26**(1), 1–15 (1990)
- Zhang, T.Y.: Effects of static electric field on the fracture behavior of piezoelectric ceramics. *Acta Mech. Sin.* **18**, 537–550 (2002)
- Pak, Y.E.: Crack extension force in a piezoelectric material. *J. Appl. Mech.* **57**(3), 647–653 (1990)
- Suo, Z., Kuo, C.-M., Barnett, D.M., Willis, J.R.: Fracture mechanics for piezoelectric ceramics. *J. Mech. Phys. Solids* **40**(4), 739–765 (1992)
- Kwon, S.M., Lee, K.Y.: Eccentric crack in a rectangular piezoelectric medium under electromechanical loadings. *Acta Mech.* **148**, 239–248 (2001)
- Sosa, H.: On the fracture mechanics of piezoelectric solids. *Int. J. Solids Struct.* **29**(21), 2613–2622 (1992)
- Liu, L.L., Feng, W.J., Ma, P., et al.: Fracture analysis of a penny-shaped dielectric crack in a piezoelectric cylinder. *Acta Mech.* **226**, 3045–3057 (2015)
- Pak, Y.E.: Linear electro-elastic fracture mechanics of piezoelectric materials. *Int. J. Fract.* **112**(1), 79–100 (1992)
- Yang, P.S., Liou, J.Y., Sung, J.C.: Subinterface crack in an anisotropic piezoelectric bimaterial. *Int. J. Solids Struct.* **45**, 4990–5014 (2008)
- Ou, Z.C., Chen, Y.H.: Near-tip stress fields and intensity factors for an interface crack in metal/piezoelectric bimaterials. *Int. J. Eng. Sci.* **42**, 1407–1438 (2004)
- Govorukha, V., Kamlah, M., Sheveleva, A.: Influence of concentrated loading on opening of an interface crack between piezoelectric materials in a compressive field. *Acta Mech.* **226**, 2379–2391 (2015)
- Li, S.F., Mataga, P.A.: Dynamic crack propagation in piezoelectric materials-part I. Electrode solution. *J. Mech. Phys. Solids* **44**(11), 1799–1830 (1996)
- Li, S.F., Mataga, P.A.: Dynamic crack propagation in piezoelectric materials-part II. Vacuum solution. *J. Mech. Phys. Solids* **44**(11), 1831–1866 (1996)
- Narita, F., Shindo, Y.: Dynamic anti-plane shear of a cracked piezoelectric ceramic. *Theor. Appl. Fract. Mech.* **29**(3), 169–180 (1998)
- Gu, B., Wang, X.Y., Yu, S.W., Gross, D.: Transient response of a Griffith crack between dissimilar piezoelectric layers under anti-plane mechanical and in-plane electrical impacts. *Eng. Fract. Mech.* **69**, 565–576 (2002)
- To, A.C., Li, S., Glaser, S.D.: On scattering in dissimilar piezoelectric materials by a semi-infinite interfacial crack. *Q. J. Mech. Appl. Math.* **58**(2), 309–331 (2005)
- Gao, C.F., Wang, M.Z.: Collinear permeable cracks between dissimilar piezoelectric materials. *Int. J. Solids Struct.* **37**, 4969–4986 (2000)
- Chi, S., Chung, Y.L.: Cracking in coating-substrate composites with multi-layered and FGM coating. *Eng. Fract. Mech.* **70**, 1227–1243 (2003)
- Sedaghati, R., Dargahi, J., Singh, H.: Design and modeling of an endoscopic piezoelectric tactile sensor. *Int. J. Solids Struct.* **42**, 5872–5886 (2005)

22. Wang, Y.C., Chen, Y.W.: Application of piezoelectric PVDF film to the measurement of impulsive forces generated by cavitation bubble collapse near a solid boundary. *Exp. Therm. Fluid Sci.* **32**, 403–414 (2007)
23. Ding, S.H., Li, X.: Periodic cracks in a functionally graded piezoelectric layer bonded to a piezoelectric half-plane. *Theor. Appl. Fract. Mech.* **49**, 313–320 (2008)
24. Peng, X.L., Li, X.F.: Transient response of the crack tip field in a magneto-electroelastic half-space with a functionally graded coating under impacts. *Arch. Appl. Mech.* **79**, 1099–1113 (2009)
25. Asadi, E., Fariborz, S.J., Fotuhi, A.R.: Anti-plane analysis of orthotropic strips with defects and imperfect FGM coating. *Eur. J. Mech. A/Solid.* **34**, 12–20 (2012)
26. Ding, S.H., Li, X.: The collinear crack problem for an orthotropic functionally graded coating-substrate structure. *Arch. Appl. Mech.* **84**, 291–307 (2014)
27. Bayat, J., Ayatollahi, M., Bagheri, R.: Fracture analysis of an orthotropic strip with imperfect piezoelectric coating containing multiple defects. *Theor. Appl. Fract. Mech.* **77**, 41–49 (2015)
28. Zhang, Y.N., Li, J.L., Xie, X.F.: Dynamic propagation characteristics of a mode-III interfacial crack in piezoelectric bi-materials. *Adv. Mater. Sci. Eng.* **1**, 1–21 (2022)
29. Hu, S.S., Liu, J.S., Li, J.L.: Fracture analysis of griffith interface crack in fine-grained piezoelectric coating/substrate under thermal loading. *Adv. Math. Phys.* **1**, 1–15 (2020)
30. Chen, H.S., Wei, W.Y., Liu, J.X., Fang, D.N.: Propagation of a semi-infinite conducting crack in piezoelectric materials: Mode-I problem. *J. Mech. Phys. Solids* **68**(1), 77–92 (2014)
31. Li, X.F., Tang, G.J.: Transient response of a piezoelectric ceramic strip with an eccentric crack under electromechanical impacts. *Int. J. Solids Struct.* **40**, 3571–3588 (2003)
32. Wang, X.Y., Yu, S.W.: Transient response of a crack in piezoelectric strip subjected to the mechanical and electrical impacts: mode-III problem. *Int. J. Solids Struct.* **37**, 5795–5808 (2000)
33. Wang, B.L., Han, J.C., Du, S.Y.: Dynamic response for non-homogeneous piezoelectric medium with multiple cracks. *Eng. Fract. Mech.* **61**, 607–617 (1998)
34. Li, X.F.: Transient response of a piezoelectric material with a semi-infinite mode-III crack under impact loads. *Int. J. Fract.* **111**(2), 119–130 (2001)
35. Noble, B.: *Methods based on the Wiener-Hopf technique*. Pergamon Press, New York (1958)
36. Freund, L.B.: *Dynamic fracture mechanics*. Cambridge University Press, Cambridge (1990)

Publisher's Note Springer Nature remains neutral with regard to jurisdictional claims in published maps and institutional affiliations.

Springer Nature or its licensor (e.g. a society or other partner) holds exclusive rights to this article under a publishing agreement with the author(s) or other rightsholder(s); author self-archiving of the accepted manuscript version of this article is solely governed by the terms of such publishing agreement and applicable law.